UNIVERSITY OF CALIFORNIA
RIVERSIDE

Regulation of the Physical Niche to Guide Human Induced Pluripotent Stem Cell Behaviors

A Thesis submitted in partial satisfaction
of the requirements for the degree of

Master of Science

in

Bioengineering

by

Robyn Jane Goodrich

June 2022

Thesis Committee:
Dr. Jin Nam, Chairperson
Dr. Boris Hyle Park
Dr. Joshua Morgan

The Thesis of Robyn Jane Goodrich is approved:

_____

_____

_____

Committee Chairperson

University of California, Riverside

ACKNOWLEDGEMENTS

I would first like to start off by acknowledging and thanking my research advisor, Dr. Jin Nam. With all his knowledge and expertise in mechanotransduction, biomaterials, and stem cell research, he has helped me excel as a researcher and an engineer. He also has really prepared me with so many valuable techniques that I will definitely apply to my future career. Despite covid and having half of my graduate studies online, I was able to learn so much by doing research in lab and under Dr. Nam's guidance, I was able to accomplish so much.

I would also like to thank our collaborators, Dr. Yadong Yin and Zuyang Ye for synthesizing the nanoparticles needed for my chapter 3 as they were an integral part of that project. I would like to also thank my thesis defense committee members, Dr. Joshua Morgan and Dr. B. Hyle Park for taking their time and agreeing to evaluate my defense.

Next, I would like to thank my fellow colleague, Youyi Tai, for tolerating my constant pestering. He has helped me a lot such as; settling in the lab, learning new techniques needed for my research, and for being just a good friend. Finally, I would like to thank my family for their endless support and for driving me to excel with everything I do.

ABSTRACT OF THE THESIS

Regulation of the Physical Niche to Guide Human Induced Pluripotent Stem Cell Behaviors

by

Robyn Jane Goodrich

Master of Science, Graduate Program in Bioengineering
University of California, Riverside, June 2022
Dr. Jin Nam, Chairperson

Mechanotransduction is a process in which cells convert mechanical stimuli into a cellular response to compensate to a dynamically changing mechano-microenvironment. The stem cell niche isn't constant, during morphogenesis various dynamic mechanical cues lead to the subsequent differentiation of germ layer specific cells, resulting in the development of specific tissues. When muscular movement is restricted in embryos, they are unable to make any movement needed for muscle development leading to issues in skeletal development. This demonstrates that the dynamic physical microenvironment is integral in embryonic development in driving lineage commitment to regulate tissue morphogenesis. In this regard, the current work focused on examining the effects of the physical mechano-microenvironment, using electrospun scaffolds and developing a

dynamic magneto-modulated hydrogel, to examine the cellular behaviors of human induced pluripotent stem cells (iPSCs). We examined the effects of the physical mechano-microenvironment on (1) Rho-ROCK-YAP signaling as well as (2) directed multilineage differentiation. By culturing iPSCs on electrospun nanofibrous scaffolds, three-dimensional (3D) colonies are able to form where the spatially localized activity of Rho-ROCK signaling leads to the activation of Yes-associated-protein (YAP) which leads to the subsequent epigenetic histone marker expression. We further demonstrate that the activation of ROCK in iPSCs under differentiation condition causes more mesendodermal expression on outer layers of colonies while ectodermal markers are localized inside the colonies. Finally, we demonstrate that the mechano-modulation of scaffold stiffness leads to activation of Rho-ROCK signaling under higher stiffness while analyzing how anisotropic stiffness affects iPSC cell morphology as well as enhancing lineage specific differentiation of iPSCs. Overall, these findings demonstrate the integral role that Rho-ROCK-YAP signaling plays in mechanotransduction and how the physical niche of stem cells can be manipulated to better control iPSC colony morphology and differentiation efficiency to best mimic *in vivo* human gastrulation. We also demonstrate that our magneto-responsive hydrogel has dynamic capabilities that can be utilized towards more specified tissue morphogenesis and for further studies of iPSC behavior in response to the changing physical microenvironment.

TABLE OF CONTENTS

LIST OF FIGURES

CHAPTER 1. LITERATURE REVIEW

1.1- Stem Cell Mechanobiology and Enabling Technology for its Investigation

It has been shown throughout studies of embryonic development that mechanical cues drive stem cell differentiation toward specific lineages[5]. Similarly, matrix stiffness and dynamic mechanical forces have been also shown to influence stem cell differentiation and the cellular response to its microenvironment in vitro[5, 6]. For example, stem cells cultured on a softer substrate, a stiffness similar to brain tissue, will spontaneously differentiate more towards neurons while cells cultured on stiffer substrates similar to bone will differentiate towards an osteogenic lineage[7]. Dynamic mechanical forces can also have an effect on stem cell behavior since the dynamic physical environment is integral in regulating the self-renewal and differentiation of stem cells[8]. In this regard, synthetic matrices, such as hydrogel systems and electrospun scaffolds, can be used to precisely control biophysical properties of the stem cell niche as well as demonstrate how the mechanical cues, such as stiffness and viscoelasticity, have an effect on stem cell migration, proliferation, and differentiation[8, 9]. The versatility of functional polymeric scaffolds that are able to recapitulate the various biophysical properties of the stem cell niche is described in **Figure 1.1**[1]

1.1.1. – The effects of matrix stiffness on stem cell behaviors

During embryogenesis, the dynamic regulation of cellular microenvironments is a key mechanism in directing stem cell differentiation and subsequent tissue morphogenesis. Tissue morphogenesis is brought about by spatiotemporal coordination of chemical and mechanical signals in multicellular organisms, therefore with a dynamically changing environment, the material properties determine how the developing cells will respond and differentiate according to the ever changing the microenvironment or stem cell niche[10, 11]. Through the utilization of various types of substrates, such as polymeric scaffolds, that closely resemble the extracellular matrix (ECM)-like morphology of the stem cell environment, stem cell differentiation can be investigated by isolating those specific biophysical properties.

There have been many studies that demonstrate the effects that substrate stiffness has on pluripotent stem cells. In a study done by Kim et al. a stiffness gradient using polyvinyl alcohol (PVA) hydrogel was used to specifically investigate stem cell behaviors[12]. By having a stiffness gradient of around 1kPa up to 24kPa along their PVA hydrogel, bone marrow stem cells were able to either promote neurogenesis along the softer region while osteogenesis was promoted along the stiffer region of the hydrogel[12]. This indicates the integral role that the physical mechanical environment has on stem cell differentiation. In addition to hydrogel systems, electrospun scaffolds have been particularly useful to regulate stem cell behaviors by their precise control over substrate stiffness. For example,

Maldonado et al. studied how engineering human induced pluripotent stem cell (iPSC) colony dimensionality using electrospun scaffolds with various mechanical properties enhances lineage specific differentiation efficiency[2]. Through the utilization of different types of polymeric electrospun scaffolds with varying fiber diameters and stiffnesses, they found that iPSCs cultured on a stiffer scaffold differentiated towards the mesendodermal lineage while iPSCs cultured on softer scaffolds exhibited a greater tendency to differentiate towards the ectodermal lineage[2]. Such electrospun scaffold stiffness-dependent differentiation behaviors were regulated by the differential formation of colony morphology; iPSCs cultured on a softer substrate tended to form 3D colonies while iPSCs cultured on a stiffer substrate tended to take up more surface area and form 2D like colonies (**Figure 1.2)**.

Another study that demonstrates how matrix stiffness can affect stem cell differentiation is through the work of Zhu et al., where how matrix stiffness modulates the differentiation of neural crest stem cells (NCSCs) is investigated in vivo. Since stem cells are often transplanted with scaffolds for tissue regeneration, it's important to be able to resemble the mechanical properties of the specific tissue that needs repair. In this case, Zhu et al. differentiated iPSCs into NCSCs and then embedded them into polyacrylamide (PA) hydrogel on the outer surface of nanofibrous polymer grafts and then implanted them into rat carotid arteries[13]. Ultimately, they found that the NCSCs cultured on the outer surface of the polymer grafts (stiffer region) differentiated into smooth muscle cells while NCSCs cultured

more inside the hydrogel (softer region) differentiated into glial cells. Their results exemplify how a scaffold's mechanical properties play an important role in directing stem cell differentiation in vivo, demonstrating the significance of biomaterial design for regenerative therapies[13]. Furthermore, pluripotent stem cells cultured on substrates with varying stiffness have shown to possess diverse lineage commitment in response to the mechanical stimuli sensed by the cells[14]. This lineage commitment in response to the stiffness change is due to intracellular signaling through mechanotransducers Rho Kinase (ROCK) which is in charge of modulating important cell functions, such as motility, dynamic reorganization of the actin cytoskeleton assembly which in turn affects stem cell differentiation[14, 15].

1.1.2. – The effects of dynamic mechanical forces on stem cell behaviors

Culturing stem cells on substrates of varying stiffness leads to lineage/phenotype-specific stem cell differentiation, depending on what tissue stiffness the substrate is relative to. During embryogenesis, however, a dynamically changing environment, varying stiffness as embryogenesis occurs, ultimately determines stem cell fate. Although most developmental biology studies focus on chemical and biological factors governing stem cell differentiation, physical forces play an integral role on embryo development; stem cells experience forces from neighboring cells and/or remote tissues and then transduce those forces into biochemical signals[16]. Specifically, the development of stem cells is determined by environments that provide a plethora of physical cues, including

mechanical forces that shape the microenvironment[16, 17]. Mechanical forces such as tensile loads and shear stresses are known to induce changes in the morphology and fate of stem cells[18]. Many studies have shown various methodologies on how to simulate dynamic mechanical forces on stem cells. These include simulating the mechanical forces by utilizing multifunctional scaffolds that respond to various exogenous stimuli such as direct mechanical, electrical, and/or magnetic factors.

1.2– Cell culture platforms for the regulation of mechanical microenvironment

There are many cell culture platforms that are currently being used to regulate the mechanical microenvironment of cells. These platforms can either be used to culture cells in two-dimensional (2D) or three-dimensional (3D). 2D monolayer culture systems have typically been used as in vitro models to study cellular responses to stimulations such as biophysical and biochemical cues[19]. Although 2D cell culture systems have been primarily used in the understanding of cellular physiology due to their easy-to-use characteristics, 3D cell culture systems provide superior properties, especially resembling in vivo conditions[19, 20]. 3D culture systems induce the cells to form aggregates or spheroids within a matrix, or on a matrix, or in a suspension medium which allows for better cell-cell interactions and cell-ECM interactions that closely mimic the cellular microenvironment found in vivo[21]. Juxtaposed with these systems, static and dynamic mechanical conditions

can also be applied to regulate cellular microenvironments. Static conditions include seeding cells on top of an electrospun scaffold or even culturing cells within a hydrogel system, both of which having designed mechanical properties. Dynamic conditions include both aspects with the caveat of incorporating extrinsic factors that can further dynamically control the microenvironmental conditions. These culture conditions are enabled by the use of various multi-functional scaffolds such as mechano-responsive polymeric scaffolds, conductive polymeric scaffolds, nanoparticles embedded in polymeric scaffolds as well as magneto responsive polymeric scaffolds.

1.2.1 – Cell culture systems for static mechanical microenvironment

1.2.1.1 – Electrospun Scaffold Systems

Electrospinning is a polymer processing technique that produces nanofibrous structure, mimicking the sub-micron features of native extracellular matrix. It has been gaining popularity in tissue engineering due to its applicability for a variety of natural and synthetic polymers[22]. The electrospinning process involves utilizing the balance between the attractive and repulsive forces of charged polymeric molecules to generate polymer fibers[23]. An electrospinning setup typically consists of a capillary in which the polymer solution to be electrospun is forced; a high voltage source with positive or negative polarity, which then supplies electrical charges into the solution; and a grounded collector[23]. A syringe pump forces the

flow of a polymer solution through a capillary while the electric field created by the repulsive interactions from the collector and syringe tip, elongates the pendant drop at the tip of the capillary[23]. By regulating various electrospinning conditions such as voltage, concentration of polymer solution, humidity, needle diameter, etc. the morphological characteristics of the polymer fibers can be controlled, which subsequently affect the cellular response.

A substrate platform that is able to manipulate the mechanical cellular environment are fibrous scaffolds which can be synthesized by electrospinning and has been shown to guide cell proliferation and differentiation due to the nanofibrous morphology that is able to mimic the native ECM[24]. For example, in a study done by Maldonado et al., how the stiffness of electrospun substrates mediates cell colony morphology, subsequently affecting the self-renewal of human iPSCs was investigated[25]. Various electrospun substrates with different physicochemical properties were synthesized using different polymer precursors and surface modifications. They found that the surface chemistry significantly affected the cell colony morphology by governing the colony edge propagation. When the surface chemistry of the substrates were uniformly controlled by collagen conjugation, the stiffness of the substrate was inversely related to the sphericity of the colony[25]. This demonstrates that electrospun substrates can be used to mimic the mechanical properties of the cells along with surface modifications to improve and modulate iPSC self-renewing capabilities.

Among various morphological features, electrospun fiber alignment is essential in determining how certain cells respond, and for stem cells, how the cells differentiate. Lin et al. conducted a study on the interaction of iPSC-derived neural stem cells on poly(L-lactic acid) (PLLA) nanofibrous scaffolds for their potential use in neural tissue engineering[26]. In this study, they used mouse iPSCs and differentiated them into neural stem cells (NSCs) where they seeded them onto aligned PLLA nanofibers and randomly oriented PLLA nanofibers. For both conditions, they assessed their cytocompatibility as well as their neurite guidance effect on NSCs. They found that the aligned PLLA fibers promoted the adhesion, survival, growth and proliferation of the NSCs in comparison to the randomly oriented PLLA nanofibers which shows that the morphology of the aligned fibers greatly directed neurite outgrowth and significantly promoted neurite growth of NSCs along the fibers[26]. This is a prime example demonstrating how electrospun fiber alignment can affect stem cell fate. Another study that shows the effects of utilizing an electrospun scaffold is through the work of Mahboudi et al[27]. In this study, human iPSCs were cultured on polyethersulfone (PES) nanofiber scaffolds while another condition consisted of iPSCs cultured using a scaffold free method. In order to observe whether the microenvironment provided by the electrospun PES scaffold enhanced chondrogenesis, real-time PCR was performed to evaluate the cartilage-specific genes in the mRNA levels. They found that there was significant expression of chondrogenic genes such as aggrecan, collagen type II and collagen type X on the PES cultured human iPSCs in comparison to those

measured in the scaffold free method[27]. This study shows that the differentiation behavior of iPSCs can be regulated by using an electrospun scaffold with characteristics similar to that of the chondrogenic environment. By mimicking the extracellular microenvironment of the native ECM, therefore, stem cell differentiation can be regulated into the desired cell type.

1.2.1.2 - Hydrogel Systems

Hydrogel systems have become increasingly popular platforms for the 3D cultivation of mammalian cells. The versatility of hydrogel materials enables the development of cell culture platform predefined with desired mechanical properties and biofunctionality[3]. Hydrogels possess essential properties that are desirable for studying cell behaviors; including that they are biocompatible, that they can be biochemically and mechanically controllable by exploiting the presentation of cell adhesive epitopes or even by changing the hydrogel crosslinking density[3, 28]. Hydrogels also possess the capability to mimic the ECM since they present similar viscoelastic and diffusive transport properties that can both be modified mechanically and biochemically[28]. Since native tissue requires the exchange of molecules between organelles, cells, or organisms and their environment, hydrogels capable of achieving diffusivity of selected molecules also make it a valuable platform of studying cells in vitro[29]. The figure (**Figure 1.3**) below demonstrates how the source, crosslinking type, and design features of hydrogels are classified to modulate the overall physicochemical properties of the system.

Many studies have demonstrated the capabilities of hydrogel for recapitulating the cellular microenvironment. One example that demonstrates this is through the work of Wu et al., where three-dimensional hyaluronic acid hydrogel-based models were developed for in vitro human iPSC-derived neural progenitor cells (NPC) culture and differentiation[30]. In this study they utilized a 3D methacrylated hyaluronic acid (Me-HA) hydrogel for the encapsulation of human iPSC-NPCs as an in vitro culture model and further investigated the role of the hydrogel rigidity on stem cell differentiation. It was found that the HA-based hydrogel's soft matrix promotes neural differentiation of human iPSC-NPCs and is an effective 3D model for central nervous system disease studies[30]. In addition, Luo et al. studied how three-dimensional hydrogel culture conditions promote the differentiation of human induced pluripotent stem (hiPSCs) cells into hepatocytes, where the derivation of hepatocyte-like cell (HLC) spheroids in the hydrogel may provide a foundation for drug screening and hepatocyte transplantation[31]. These studies demonstrate the versatility of hydrogel and its applicability in studying cells in 3D for a better understanding of cells and their response to various conditions.

1.2.1.3 - PDMS microarrays

Polydimethylsiloxane (PDMS) is an elastomer that has been widely used for both industrial and biomedical applications due to it numerous advantages such as; biocompatibility, flexibility, stability over a wide range of temperatures, gas permeability, and optical transparency[32, 33]. Therefore, PDMS has been widely

used as a platform for a better understanding of cellular behavior. For micro-scale patterning of cells, microarrays can be used to influence cellular alignment and shape. Typically the molecules of interest are adsorbed onto a PDMS stamp and then transferred to a chemically activated substrate by direct contact of the substrate with the stamp while areas without these micro-patterns are treated through plasma etching to inhibit cell adhesion[34].

In addition, PDMS microarrays can be used to study iPSC behavior. For example, Lee et al. did a study on highly efficient reprogramming and characterization of iPSCs by using microwell arrays[35]. To do this the researchers compared using a basic tissue culture plate to using a well-defined culture system based on a PDMS stencil. They found that the system using the PDMS stencil was able to support the efficient reprogramming of fibroblasts into iPSCs[35]. They ultimately found that the human fibroblasts cultured on the PDMS stencil supported the reprogramming of the human fibroblasts to pluripotency which had a 5-fold higher efficiency compared to the conventional tissue culture plate method. This was ultimately due to the PDMS stencil providing a more even distribution and transduction of the 4-defined viral vectors to the fibroblasts which enabled better reprogramming of the fibroblasts to iPSCs[35]. In addition to this, another study by Tran et al. also demonstrates the affects that PDMS microarrays can have on cellular behavior. They studied on how controlled clustering enhances pancreatic endocrine transcription factor (PDX1 and NKX6.1) expression in pancreatic endoderm cells derived from pluripotent stem cells. During this study the

researchers cultured adherent induced pluripotent stem cell derived pancreatic foregut (PF) cells on a micropatterned PDMS surface and demonstrated that sufficiently small patterns can prompt clustering into multilayered structured during the pancreatic endoderm (PE) transition. Ultimately, they found that the microwell system was able to lead to a robust system that prompted clustering, increased the cell density, and increased nuclear accumulation of PDX1 and NKX6.1[36]. This work shows that there's improved pancreatic differentiation which demonstrates that the cell-adhesive micropatterns can provide a facile, scalable and more reproducible manufacturing route to drive morphogenesis and develop well-differentiated pancreatic cell clusters[36]. PDMS microarrays allow for the manipulation of the cellular environment by allowing even distribution and efficient differentiation of iPSCs towards specific lineages.

1.2.2 - Cell culture systems for static mechanical microenvironment

1.2.2.1 - Mechano-Responsive scaffolds

In vivo, dynamically changing environments affect the embryo development and its subsequent tissue specification. These cellular responses are highly dependent on anatomical location and the cell's developmental stage. In vitro, a substrate's mechanical properties can play a crucial role in manipulating cellular behaviors. Those mechanical properties include tensile strength, elastic modulus, and fracture toughness in both macroscopic and microscopic scales which exert a

significant impact on cells in a magnitude-dependent manner[1]. In addition to these static conditions, exogenous mechanical stimulation has become an increasingly effective modality in directing stem cell proliferation and differentiation[37]. Therefore, utilizing mechanically tuned scaffolds would provide a platform to both extrinsically (i.e., applied forces) or intrinsically (i.e., substrate stiffness) control the mechanical environment of the cells to achieve the desired cellular responses[1].

A fibrous scaffold can be utilized to enhance biomechanical forces that result in changes in stem cell behavior. For example, in a study done by Horner et al. electrospun three-dimensional scaffolds were used to culture human mesenchymal stem cells (hMSCs) to various magnitudes of dynamic compressive strains[38]. It was found that gene expression of chondrogenic markers were upregulated in response to increased magnitudes of compressive strain while osteogenic markers had noticeable decreased due to the compressive loading[38]. This demonstrates how mechanical stimulation has an effect on stem cell differentiation and stem cell fate. Stem cell differentiation varies as the dynamic stimulus is altered in response to the change in the mechano-environment.

In the work done by Bryant et al., they focused on how crosslinking density can influence the morphology of chondrocytes photo-encapsulated in poly(ethylene glycol) (PEG) hydrogels during the application of compressive strain. They found that the crosslinking density of the hydrogel scaffold can influence the morphology of encapsulated chondrocytes in response to an applied mechanical load. By using a higher density, they were able to obtain a 11-fold higher compressive modulus

as well as achieve heterogenic cell deformation, which varied depending on those densities[39]. This study demonstrates that by altering the crosslinking densities, different levels of cartilage ECM regeneration could be engineered[39]. In summary, mechano-responsive scaffolds have various applications in tissue engineering and regenerative medicine, especially for mechano-sensitive tissues in the musculoskeletal system, and have and will be continuing to be making headway towards directing cellular behaviors and guiding stem cell differentiation.

1.2.2.2 – Magneto responsive polymeric scaffolds

Among various physical factors, magnetic fields have also shown to affect cellular behaviors[33, 40, 41]. Magnetic nanoparticles (MNPs) provide a means to safely apply magnetic fields to cells in vitro and in vivo. Such magnetic fields can be precisely controlled by using ferromagnetic or superparamagnetic properties that can permanently or temporally magnetized under exogenously applied magnetic fields[41].

It has been shown that encapsulating ferromagnetic MNPs in a polymeric scaffold can aid in promoting the proliferation of the adherent cells and enhancing their cellular activities. For example, Kim et al. performed a study on how magnetic scaffolds of PCL with functionalized magnetite nanoparticles are able to manipulate the physicochemical, mechanical, and biological properties for bone regeneration[42]. Magnetite iron oxide (Fe_3O_4) nanoparticles were functionalized through surfactant mediation, to improve their hydrophilicity, and then were

encapsulated into a PCL polymeric scaffold. The MNPs incorporated into those scaffolds demonstrated to promote the mineral formation while exhibiting good tissue compatibility[42]. For the dynamic control of the magnetic microenvironment, Chen et al[4]. showed MNP's capabilities to provide a microenvironment to enhance cellular activity, where magnetic stiffening through the usage of iron oxide nanorods in hydrogel was studied to analyze the effects this microenvironment on epithelial cells. The study used magnetic nanorods (MNRs) imbedded in polyisocyanide (PIC)-based hydrogels and utilized permanent magnetics to apply magnetic fields to induce stiffening to the hydrogel. They found that due to the magnetic stiffening, the 3D epithelial cell cultured on top of the magnets gave rise to a change in cellular morphology which was shown as the MCF10A colonies became more spread out in comparison to the non-magnetic condition[4]. These forces that were generated due to the magnetic field and strain of the MNRs allow for the mimicry of contractile forces typically found in biology, giving real time outcomes that can effect cellular development[4]. **Figure 1.4** below demonstrates how the forces exerted through the nanorods from the magnetic field affected hydrogel stiffness as well as cellular morphology. These examples showcase the anabolic effects of MNPs and MNRs when incorporated within a polymeric scaffold and allow for the promotion of cellular activities.

As described previously, both mechanical stimulation and the implementation of MNPs have been shown to modulate cellular behaviors which include migration, proliferation, and differentiation. It has been reported that a

magnetic field (MF) and/or an electromagnetic field (EMF) along with polymeric scaffolds can play significant roles in guiding cell fate and affecting the process of wound repair[43]. Magneto-responsive polymeric scaffolds by encapsulating MNPs can provide an opportunity to induce dynamic mechanical perturbation under the applied magnetic fields[44]. The high-frequency vibration of MNPs in polymeric scaffolds with a dynamically changing magnetic field would mechanically deform the substrate and stimulate adherent cells in the nano or microscale. Combining magnetic and mechanical stimulation will likely influence a series of cellular behaviors including activation of magnetic and mechanical sensitive channels, cytoskeleton reorganization, and expression of specific genes, resulting in a more controllable and accurate physical stimulation[45].

Magneto-responsive polymeric scaffolds when exposed to applied MFs have been shown to improve cellular behaviors for a wide variety of tissue engineering applications. For example, Goncalves et al. performed a study on exploring the potential of starch/PCL (SPCL) aligned magnetic responsive scaffolds for tendon regeneration[46]. They fabricated such scaffolds by incorporating iron oxide MNPs into a 3D structure of aligned SPCL fibers by rapid prototyping technology. They showed the effect of an externally applied magnetic field on tenogenic differentiation of adipose stem cells (ASCs), where the cells undergo successful tenogenic differentiation on the scaffold[46]. The implantation of the magnetic scaffolds into a rat model showed good biocompatibility and integration of the surrounding tissues, synthesizing proteins that are essential for

tenogenic development[46]. This study emphasizes the significant effects of incorporating an external magnetic field onto a MNP encapsulated polymeric scaffold. In addition, magneto-responsive scaffolds has been also shown to enhance neural regeneration. For example, Liu et al. demonstrated how a magnetically responsive nanocomposite scaffold combined with Schwann cells promotes sciatic nerve regeneration upon exposure to an external magnetic field[47]. Biodegradable chitosan-glycerophosphate polymer embedded with magnetic nanoparticles was utilized for the magnetic nanocomposite scaffold[47]. Tunable magnetization, degradation rate, as well as the maintenance of Schwann cell viability after transplantation were observed under a magnetic field, potentially suggesting the synergistic effects of direct magnetic and induced mechanical stimulation.

1.3- Conclusion

Through the discoveries and applications of the various tissue engineering methods and techniques used to simulate the physical microenvironments needed to enhance iPSC behaviors, more personalized regenerative medicine and tissue engineering techniques can be developed for future therapeutics. Electrospinning is becoming a more prominent method of generating scaffolds used to promote cell infiltration and allows versatility in manipulating the physical environment in 3D allowing for a broad range of applications versus 2D substrates. Hydrogels are also becoming an increasingly popular 3D cultivation substrate that allows for

enhanced cell encapsulation as well as resembles the desire cellular mechanical properties that aid in their biofunctionality. Through the recent development of these multifunctional polymeric scaffolds combined with the exogenously applied stimuli, including mechanical and magnetic stimulation, tissue morphogenesis as well as affective tissue regeneration can be better facilitated for regenerative therapeutics.

These discoveries and results can lead to the development of functionally mature engineered tissues *in vitro* for diagnostics, tissue repair implantation and even drug discovery platforms. Despite this, there are still a lack of systematic evaluation and control of many of these physical factors to more precisely direct cellular behaviors resulting inconsistent results among studies. In this case, a more methodical approach needs to be taken to fully cover the effects among the various parameters needed for optimal development of tissues and cells (i.e. magnitude, frequency, or duration of each physical factor). Nonetheless, the recent advances in these multifunctional polymeric scaffolds will aid in the discoveries for efficient tissue engineering constructs for clinical applications.

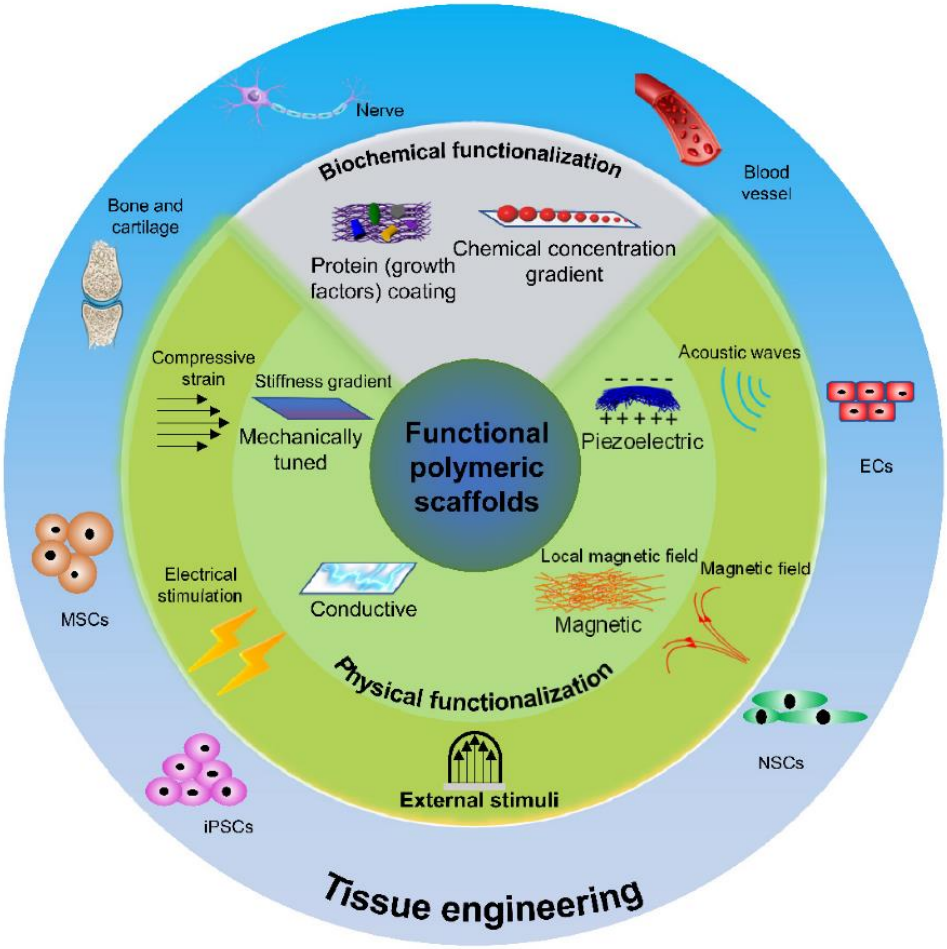

Figure 1.1. Schematic portraying the versatility of polymeric scaffolds in stem cell/tissue engineering[1]

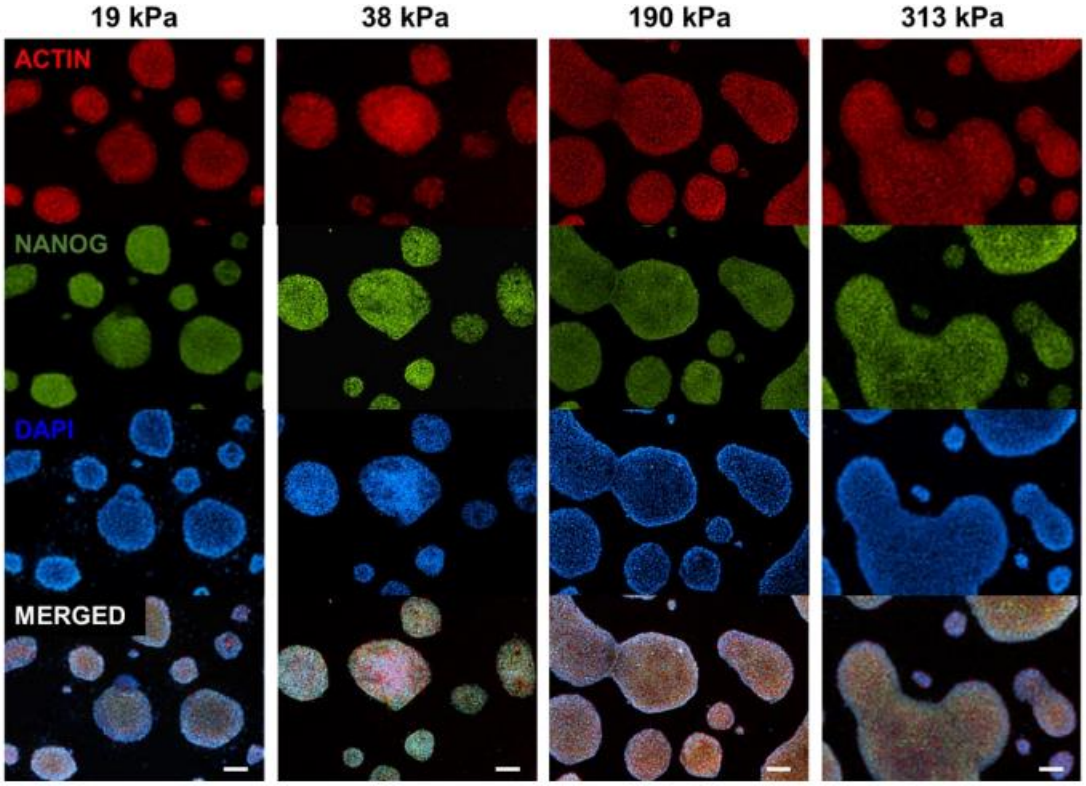

Figure 1.1. iPSCs cultured on softer substrates demonstrated 3D like colony morphologies while iPSCs cultured on stiffer substrates demonstrated 2D like morphologies while both of the conditions maintaining pluripotency (demonstrated by NANOG expression)[2]

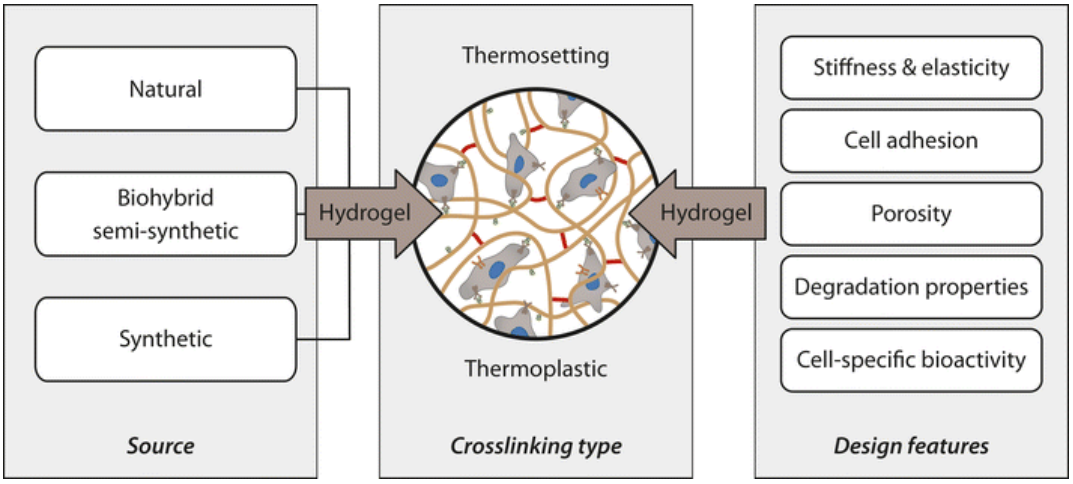

Figure 1.2. Classification of Hydrogel for 3D culture[3]

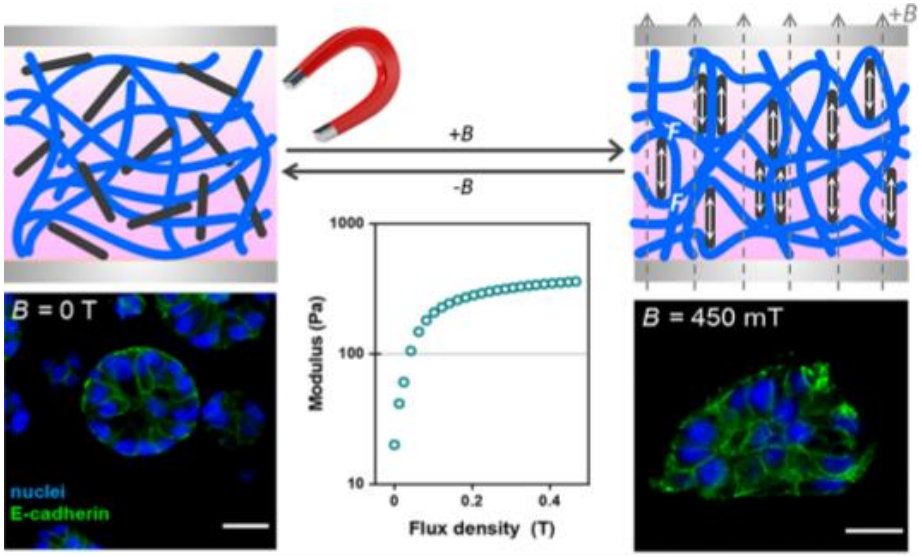

Figure 1.4. Permanent Magnetic Field affects orientation of nanorods which increase hydrogel stiffness and in turn influences cellular morphology[4]

CHAPTER 2. HETEROGENEITY REGULATION OF HUMAN INDUCED STEM CELLS THROUGH MECHANOTRANSDUCTION SIGNALING

2.1 – Abstract

Biochemical factor mediated pluripotent stem cell (PSC) differentiation have been extensively studied, but it is only recently that a critical role has been revealed for physical microenvironment in controlling PSC early lineage commitment. The mechanisms of mechanotransduction, in response to the cellular physical microenvironment and cell-cell interactions, remain unclear. In this study, nanofibrous scaffold culture system is used to engineer distinct 3D semispherical colony formation of human induced pluripotent stem cells (iPSCs) to examine spatial dependent cellular mechanical responsive signaling activities, DNA histone modifications, and germ layer differentiation. The results show that, due to the spatial differences of the physical microenvironment, the RhoA activity, accompanied by the formation of actin-myosin ring, is located in a spatially organized manner and further induces downstream YAP activation, localized epigenetic regulations, and heterogeneous germ layer differentiation. The spatially organized force as well as differentiation pattern is also confirmed by altering the 3D colony shapes. These detailed mechanotransduction observations provide a means to precisely control PSC early lineage differentiation for future therapeutic interventions and other clinical applications.

2.2 – Introduction

Stem cells possess great potential for therapeutic applications due to their differentiation capability to a variety of end phenotypes. Especially, embryonic stem cells (ESCs) and induced pluripotent stem cells (iPSCs), collectively known as pluripotent stem cells (PSCs) have been extensively investigated due to their extensive capability of self-renewal and differentiation toward phenotypes in all three germ layer lineages. Various biochemical factors based on developmental biology studies have been explored to guide the differentiation of those stem cells into specific cells/tissues with unique functionality, to develop tissue replacements for in vivo regeneration or in vitro tissues for various developmental/pathological/pharmaceutical studies[48]. For example, a sequential application of BMP4 and Activin A was demonstrated to enhance the lineage specification of iPSCs toward mesendoderm[49] while pharmaceutically inhibition of the SMAD signaling by SMAD inhibitors noggin and SB431542 was utilized to effectively guide PSC differentiation to the ectodermal lineage and subsequent neural cells[50].

In addition to the obvious contributions of biochemical factors, mechanical cues, generated by the cell-cell and cell-matrix interactions, also play important roles in regulating stem cell behaviors including morphological organization and differentiation[51, 52]. During the early stages of development, different mechanical environments experienced by the stem cells regulate or even determine the cell lineage specification. Maldonado et al. demonstrated that the stiffness of the cell

culture substrate significantly affects the colony morphology of human iPSCs and their early lineage specification[25]. Several studies have also found that human iPSCs that were engineered to form a circular colony differentiate into a radially organized pattern, having ectoderm, mesoderm, and endoderm from the center of the colony to the edge[53, 54]. The development of such patterned differentiation was found to depend on the heterogenous distribution of tensile and compressive forces within the colony[54]. Despite these novel findings, the molecular mechanisms pertaining to the mechanotransduction in PSCs for their early lineage commitment remain elusive at present, and the signaling cascades that induce the heterogenous, patterned differentiation to form the organized germ layers is unknown.

Recent mechanobiology studies in various cell types have provided pointers for the mechanotransduction mechanisms in PSC differentiation. The physical/mechanical cues perceived by cells have shown to induce cellular responses mediated through focal adhesion kinase (FAK)-Rho/ROCK (Rho-associated protein kinase) signaling pathway leading to actin/myosin contraction and cytoskeleton reorganization, ultimately regulating mechano-sensitive genes through various transcription factors[55, 56]. Among all these transcription factors, Yes-associated protein (YAP) was shown to be crucial in bridging cellular mechanotransduction and downstream cellular behaviors[57]. In addition, several studies suggest that epigenetic regulation is potentially regulated by the cellular physical microenvironment, affecting stem cell differentiation[58, 59]. Despite these

remarkable advances in stem cell mechanobiology, several limitations still exist including, 1) 2D cell culture systems that most mechanotransduction studies were based on, where the cell-substrate interaction unnaturally outweighs the cell-cell interaction, the major mode of force transmission in 3D physical microenvironment *in vivo*; 2) a lack of systematic investigation on the signaling cascades describing how iPSC colonies' mechanical microenvironment coordinates mechanosensing and subsequent early lineage differentiation.

In this study, we engineered a robust, reproducible stem cell culture system to provide the physical/mechanical support for human iPSCs to develop 3D hemispherical colonies, where individual cells within the colony experience different mechanical forces. We found that the differentiation of the cells in these colonies are significantly affected by the mechanotransduction pathway; perturbing the mechano-sensing regulators such as Rho/ROCK or their downstream effector, YAP, results in the disruption of spatially patterned iPSC differentiation toward mesendodermal and ectodermal lineages. Interestingly, we also discovered that the Rho/ROCK-YAP mechanotransduction modulates cell fate specification by directly regulating the epigenetic DNA histone modification. This non-uniform force distribution within the 3D colony and its effect on spatially organized iPSC differentiation pattern was confirmed by altering the shape of the 3D colonies.

2.3 – Materials and Methods

2.3.1 – Scaffold synthesis

Poly(ε-caprolactone) (PCL) electrospun nanofibrous scaffolds were synthesized as previously described. Briefly, the precursor solutions of 8 wt.% PCL dissolved in 5:1 trifluoroethanol-water (Sigma) were electrospun using a vertical setup. The processing parameters for the scaffold synthesis have been optimized to achieve approximately 500 nm average fiber diameters which result in a Reduced Young's Modulus of 19 kPa. For the system that induced the formation of spherical-dome shaped colonies, the electrospun PCL scaffolds were subjected to air-plasma-treatment before covered by a casted PDMS film with pre-patterned 200-μm circular hollows to induce the spherical colony formation as well as restrict the size of the cell colonies. The assembled scaffolds were cut into small circular pieces having 8 mm dimeter to fit into a 24-culture plate well. For the system that induced elliptical-dome shaped colonies, the PDMS films that covered the electrospun PCL scaffolds were firstly stretched using a tensile force generator to make elliptical hollows with an aspect ratio of 2:1. The stretching process last for 12 hours at 60 °C temperature.

2.3.2 – Cell Culture

A human patient-specific induced pluripotent stem cell line, which was derived and well characterized as previously described, was used in this study. Cells were maintained on Geltrex®-coated (Life Technologies) tissue culture

plates in proliferation media mTeSR1 (StemCell Technologies) at 37 °C and 5% CO_2. iPSCs were seeded onto the PCL scaffolds at approximately 120,000 cells cm^{-2} of scaffold. ROCK inhibitor, Y-27632 (10 μM, Reagents Direct, Encinitas, CA), was supplemented to the proliferation media to improve initial cell attachment and survival. The following day, Y-27632 was removed from the media unless otherwise noted.

To examine the effect of ROCK activity on colony morphology differentiation, iPSCs were pre-cultured in mTeSR1 medium for 5 days to allow for the development of distinct colony morphologies. Alternatively, the proliferation media was supplemented with 40 μM Y-27632 during the 5-day pre-culture period. After the pre-culture period the proliferation media was exchanged to either defined mesendoderm or ectoderm differentiation media as previously described. Briefly, the mesendoderm differentiation media consist of DMEM:F12 basal media sequentially supplemented with Activin A (Peprotech), WNT3A (R&D systems), FGF2 (R&D systems), and BMP4 (R&D systems) for 60 hours. Ectoderm differentiation was induced using the media consisting of neurobasal media (Gibco) supplemented with B27 (Gibco), N2 (Gibco), 2 μM dorsomorphin (Compound C, Sigma) and 0.1 μM retinoic acid (Sigma) for 8 days. Cells were maintained in an incubator at 37 °C and 5% CO_2 with daily media exchanges. Cells were either fixed using 4% paraformaldehyde (Sigma) or treated with RLT buffer (Qiagen) for the following protein expression of gene expression analysis.

To examine the iPSC germ layer differentiation behavior within individual colonies, iPSCs were pre-cultured for 5 days and then treated with BMP4 (40 ng mL^{-1}) for 36 hours to induce simultaneous germ layer differentiation. Differentiated 3D iPSC colonies were fixed using 4% paraformaldehyde.

To examine the relationship among RhoA/ROCK, YAP, and DNA histone modifications within 3D iPSC colonies, iPSCs were pre-cultured for 5 days. 3D iPSC colonies were treated with RhoA inhibitor (Rhosin hydrochloride, 40 µM, Tocris), ROCK inhibitor (Y-27632, 40 µM), or YAP inhibitor (verteporfin, 5 µM, Tocris) for 1, 1, or 2 hours, respectively, at the end of the 5-day pre-culture period. 3D colonies that were not treated with any molecules were used as control. Cells were then fixed using 4% paraformaldehyde.

For the elliptical-dome shaped colonies culture system, iPSCs were pre-cultured for 5 days, colonies were either fixed using 4% paraformaldehyde or treated with BMP4 for 2 days before the fixation.

2.3.3 – Immunofluorescence Staining

The fixed samples were stained following a standard immunofluorescence staining protocol. Fixed samples were permeabilized using 0.1% Triton-X in phosphate buffered saline (PBS) followed by non-specific binding sites blockage of 1% bovine serum albumin (BSA) in PBS solution. The following antibodies were then utilized: mouse anti-NANOG (Abcam), goat anti-BRACHYURY (R&D Systems), mouse anti-PAX6 (Developmental Studies Hybridoma Bank (DSHB)),

mouse anti-Active-RhoA (NewEast Bioscience), mouse anti-α-tubulin (DSHB), mouse anti-Non Muscle Myosin Light Chain (DSHB), rabbit anti-SOX2 (Cell Signaling), rabbit anti-SOX17 (Proteintech), rabbit anti-H3K4me3 (Abcam), rabbit anti-H3K9ac (Abcam), rabbit anti-H3K27ac (Abcam), rabbit anti-H3K27me3 (Abcam), rabbit anti-H3K9me (Abcam), rabbit anti-YAP-488 conjugate (Cell Signaling). Except for the YAP antibody since it was conjugated with 488 fluorescent dyes, the corresponding secondary antibodies were used: Alexa Fluor 488 donkey anti-mouse IgG (H+L), Alexa Fluor 488 goat anti-rabbit IgG (H+L), Alexa Fluor 594 goat anti-mouse IgG (H+L), or Alexa Fluor 488 donkey anti-goat IgG (H+L) (Invitrogen). The samples were then countered stained, if necessary, using phalloidin (Abcam) and DAPI (Sigma) to visualize actin and nuclei. Confocal imaging was conducted using an confocal microscope (Zeiss 800 upright).

2.3.4 – RhoA analysis

To analyze the effect of colony morphology on RhoA activity, -PSCs were pre-cultured electrospun PCL scaffolds either 3 or 5 days. The presence of active RhoA was quantified using a G-LISA quantification assay using manufacturer's instructions (Cytoskeleton). Additionally, the amount of total RhoA was quantified using a Total RhoA ELISA kit (Cytoskeleton).

2.3.5 – Gene expression analysis

To examine gene expression of lineage-specific markers, cells were lysed and total RNA was purified using an RNeasy Micro Kit (Qiagen, Valencia, CA) followed by cDNA synthesis using an iScript cDNA Synthesis Kit (Bio-Rad). Quantitative real-time PCR was performed using the following custom primers: GAPDH [5'-ATGGGGAAGGTGAAGGTCG-3' (forward) and 5'-TAAAAGCAGCCCTGGTGACC-3' (reverse)]; GSC [5'-GATGCTGCCCTACATGAACGT-3' (forward) and 5'-TACTTGGTCTCCTGGAAGAGGTT-3' (reverse)]; MIXL1 [5'-CTTTGGCTAGGCCGGAGATTA -3' (forward) and 5'-GGCAGGCAGTTCACATCTACCT -3' (reverse)]; PAX6 [5'-GAGTTCTTCGCAACCTGGCTA-3' (forward) and 5'-CTGCCCGTTCAACATCCTTAG-3' (reverse)]; NEUROD1 [5'-AAAGCCCTCTGACTGATTGCA-3' (forward) and 5'-GGACGGTTCGTGTTTGAAAGA-3' (reverse)]. The comparative threshold cycle (CT) method was used to analyze the fold change differences with GAPDH used as an endogenous control.

2.3.6 – Statistical analysis

All experiments were conducted with minimum of triplicate biological samples and data is represented as mean ± standard deviation (SD). Comparison of groups for statistical significance was determined using SPSS 115 software with

either one-way ANOVA with Tukey's HSD post-hoc or one sample student T-test. Pearson's correlation coefficient was determined to reveal bivariate correlation between two factors. Statistical significance was reported when 'p' value was less than 0.05.

2.4 – Results

In our previous study, different morphologies of iPSC colonies were formed depending on the stiffness of electrospun substrates[60]. The colony morphology significantly influenced the efficiency of directed differentiation where 3D hemispherical colonies formed on a soft, flexible substrate had a greater efficiency under biochemically directed differentiation toward ectodermal lineage[61]. In contrast, the iPSCs forming colonies with 2D, flat morphology on a stiffer substrate exhibited greater mesendodermal differentiation. To understand the role of the mechano-sensitive Rho/ROCK signaling in controlling the iPSC colony morphology as well as regulating subsequent germ layer differentiation, active RhoA was firstly quantified in iPSC colonies having 2D flat or 3D hemispherical shape morphology, obtained from culturing the cells on electrospun scaffolds with different stiffness[61] (**Figure S2.1**). Greater RhoA activity was obsesrved in 3D iPSC colonies, as compared to the 2D flat colonies (**Figure S2.1**). Interestingly, the initiation of 3D colony formation coincided a significant increase in the activation of RhoA, suggesting the role of Rho/ROCK signaling in iPSC colony formation (**Figure 2.1a**). To further determine the necessity of the RhoA/ROCK

signaling for 3D iPSC colony formation, a small molecule Y027632 (ROCK inhibitor) was administered during iPSC culture on a soft PCL electrospun scaffold. The difference in colony morphology was evident where the application of ROCK inhibitor prevented the formation of 3D colonies (**Figure 2.1b**), clearly indicated by the significant decrease of colony sphericity index (**Figure 2.1c**). It should be noted that Rho/ROCK signaling activity as well as the resulting colony morphology appears to have no direct effect on the pluripotent state of the iPSCs since most of the cells exhibited the uniform expression of NANOG (**Figure 2.1b, green color**). The effects of colony morphology regulated by Rho/ROCK was further investigated by subjecting iPSC colonies with different morphologies in the presence and absence of ROCK inhibitor to biochemically mediated directed differentiation protocols[62]. The application of ROCK inhibitor suppressed the ectodermal differentiation of the cells while enhancing their mesendodermal differentiation (**Figure 2.1d**). Corroborating with the gene expression results, greater expression of mesendodermal marker, BRACHYURY (T) (**Figure 2.1e**), and less expression of ectoderm marker, PAX6 (**Figure 2.1f**), was observed under the ROCK inhibitor condition. These observations suggest that the Rho/ROCK signaling activity in iPSCs significantly affects colony morphology and preferential differentiation fate.

Interestingly, the expression of active RhoA was confined to the outermost layers of the 3D colony (**Figure 2.2a, Figure S2.2a**), potentially indicating the spatial heterogeneity in the mechanical environment within a 3D colony. As the

activation of RhoA/ROCK signaling often affects the downstream cytoskeleton organization[63, 64], the expression pattern of α-tubulin, actin, and non-muscle myosin light chain (MLC) were analyzed. Similar to the active RhoA expression, the α-tubulin was highly localized at the outermost layers of the colony (**Figure 2.2b, Figure S2.2b**), indicating the generation of greater tension at the outer layer in the spherical colony. The coinciding radial expression pattern between active RhoA and α-tubulin suggests the regulation of cytoskeletal components by RhoA/ROCK. The expression of MLC exhibited more uniform distribution throughout the entire 3D iPSC colony as compared to the α-tubulin (**Figure 2.2c, Figure S2.2c**). The colocalization between MLC and Actin especially at the outer layers of the colony (**Figure 2.2c bottom**)**,** however, suggests actin-myosin interactions, induced by RhoA/ROCK-mediated MLC phosphorylation[65, 66]. This interaction results in the formation of actomyosin cable stabilizing the colony structure and affecting the cellular differentiation[67, 68].

To investigate the effects of spatially organized expression of RhoA and associated cytoskeleton on the differentiation of iPSCs, 3D cell colonies were subjected to BMP4 stimulation for 36 hours to induce simultaneous multi-lineage differentiation[69]. Hereinafter, the cells pre-cultured on PCL scaffolds for 5 days to form 3D colonies are noted as pre-differentiation condition (prediff.) while those subsequently subjected to BMP4 treatment after the pre-culture are noted as differentiation condition (diff.). Under the diff. condition, a unique spatially organized differentiation pattern was observed where mesodermal Brachyury (T)

and ectodermal SOX2 were radially arranged from the edge to the center of the 3D iPSC colony (**Figure 2.3a, Figure S2.3a**). The expression of endodermal SOX17 was colocalized with T, suggesting the very early stage of mesendodermal differentiation, similar to the gastrulation process (**Figure 2.3b, Figure S2.3b**)[70]. This radially organized differentiation pattern in 3D iPSC colonies is clearly notable in the location tracking date, where $SOX2^+$ cells positioned in the inner parts of the colony while T^+ and $SOX17^+$ cells were localized at the outer layers (**Figure 2.3c**). Since SOX2 is also a pluripotency marker, the absence of NANOG expression was used to confirm the loss of pluripotency under diff. condition (**Figure S2.4a-d**), indicating the ectodermal lineage of those $SOX2^+$ cells in the inner parts of the differentiated 3D iPSC colonies. Note that a similar 2D radial germ layer differentiation pattern has been observed in other studies but only on 2D pluripotent stem cell culture systems. To date, however, this radial differentiation pattern in 3D iPSC colonies is the first time that is being reported by us (**Figure 2.3d**).

Since both Rho/ROCK activity and mesoderm differentiation were localized at the outermost layers of 3D iPSC colony, we examined whether this heterogeneity of differentiation behavior was regulated by the Rho/ROCK signaling. ROCK activator, Calpeptin was simultaneously applied to the 3D iPSC colonies that were being subjected to the BMP4 induced differentiation. As shown in the confocal Z-stack images (**Figure 2.4a, b, Figure S2.5a, b**), the application of Calpeptin induced more uniform distribution of T^+ cells in the inner parts of 3D

iPSC colonies, which were localized at the outer layers in the absence of the ROCK activator. The increase in the number of cells differentiated to the mesendodermal lineage throughout the entire colony with ROCK activation indicates that ROCK activity during the formation of 3D colony predisposes the cells to differentiate toward mesendodermal lineage under BMP4 stimulation (**Figure 2.4c**). This result was consistent with a previous study showing that RhoA activity is required for mesoderm development through activating actin-myosin interaction[70, 71].

Based on the observation of differentiation pattern regulated by the localized activation of Rho/ROCK, developed during the formation of 3D colonies, the epigenetic histone modification within the 3D iPSC colonies was studied to further uncover the mechanism of this physical microenvironment-mediated mechanotransduction controlling iPSC differentiation. Confocal imaging showed that the histone modification markers of transcriptional activators including trimethylation of histone H3 at lysine 4 (H3K4me3), acetylation of histone H3 at lysine 9 (H3K9ac) and lysine 27 (H3K27ac) were localized at the outmost layers of the colonies (**Figure 2.5a-c, f, Figure S2.6a-c**) while gene repressors including trimethylation of histone 3 at lysine 27 (H3K27me3) and methylation of histone 3 at lysine 9 (H3K9me), were more uniform distributed within prediff. 3D iPSC colonies (**Figure 2.5d-f, Figure S2.6d, e**). These results suggest that the activators of histone modification are potentially mechanical responsive that were regulated by the spatial-dependent mechanical cues of the 3D iPSC colonies. To confirm the mechano-sensitivity of the epigenetic modification, we next examined

the relationship between the activators of histone modification and YAP, which plays a crucial role in cellular mechanotransduction[72, 73]. The expression patterns of YAP and epigenetic markers H3K4me3 and H3K27ac were first examined in 2D iPSC colonies cultured on regular tissue culture plates. A uniform expression of both YAP and histone modification markers were observed within nuclei, indicating the activation of YAP signaling and H3K4me3 and H3K27ac histone modifications (**Figure S2.7**). Within 3D iPSC colonies, however, YAP and histone markers expressed in a confined region of the cells at the outermost layers while minimal expression was observed in the inner parts of the colonies (**Figure 2.6a, c, e, g, Figure S2.8a, c**). The application of a YAP inhibitor, Verteporfin induced the loss of YAP and H3K4me3/H3K27ac expression, indicating that YAP signaling regulates the activators of histone modification of H3K4me3 (**Figure 2.6b, d, f, h, Figure S2.8b, d**). Collectively, these results demonstrate that the spatially organized heterogeneity of epigenetic histone modification is mediated by YAP signaling, corroborating with the previous study showing a close relationship between YAP/TAZ signaling activity and epigenetic behaviors[59, 74].

As shown **Figure 2.2**, we observed a close relationship between RhoA/ROCK activity and cytoskeletal organization, likely due to the heterogeneity of mechanical microenvironment within 3D iPSC colonies. We next examined if RhoA/ROCK activity regulates YAP signaling that determined localized epigenetic modification. Prediff. 3D iPSC colonies were subjected to various conditions including stimulation with a RhoA inhibitor (Rhosin hydrochloride), a ROCK

inhibitor, and a YAP inhibitor. While YAP and active RhoA exhibited localized expression at the outermost layers of 3D iPSC colonies under normal culture condition (**Figure 2.7a, e, Figure S2.8a**), the treatment of RhoA inhibitor or downstream ROCK inhibitor caused a significantly decreased expression level of both YAP and Active-RhoA with no YAP nuclear translocation (**Figure 2.7b, c, f, g, Figure S2.8b, c**). Note that the decreased Active-RhoA level by ROCK inhibitor is probably due to the positive feedback control between RhoA and ROCK, where the inhibition of downstream ROCK will activates the Rac1, resulting in the inhibition of RhoA[75]. When iPSCs were treated with the YAP inhibitor, however, only the expression and nuclear localization of YAP were abolished while the Active-RhoA expression was still maintained at the outer layers of the 3D colonies (**Figure 2.7d, h, Figure S2.8d**), indicating that YAP does not significantly affect the RhoA/ROCK activity in 3D iPSC colonies. Thus, we confirmed that RhoA/ROCK acts upstream of YAP signaling potentially through the mediated cytoskeleton organization.

The presented results have collectively shown a spatial regulation of iPSC differentiation, mediated through a mechano-sensitive RhoA/ROCK-YAP-epigenetic modification signaling axis, where cells experience greater stresses at the outer layers of the 3D colonies as compared to the cells that were located at the inner layers. To further confirm if this patterned, heterogeneous differentiation was indeed controlled by the mechanical microenvironment, we modified our iPSC culture system utilizing PDMS-PCL scaffold construct to control the morphology of

iPSC colonies (**Figure 2.8a**). Due to physical constriction, iPSCs grown in this modified scaffold formed elliptical shaped colonies. As shown by others[76, 77], cells located at the two sharp edges of the elliptical colonies experience greater stresses, evident by the localized expression of active RhoA and YAP while minimal expression of those mechano-mediators at the long edges of the colonies (**Figure 2.8b, c, d, f, g**). As expected, both YAP and histone modification markers, H3K4me3 and H3K27ac, followed the same expression pattern of active RhoA (**Figure 2.8b, c, d, f, g**). The location-dependent heterogeneous differentiation matched the expression pattern of these mechano-mediators and epigenetic modifiers, where mesodermal marker T was localized at the outermost layers of sharp edges (**Figure 2.8e, h**).

2.5 – Discussion

Cells consistently interact with neighboring cells/tissues and the extracellular matrix, and they are stimulated by evolving physicochemical cues. Biochemical signals such as growth factors, cytokines, hormones, and signaling mediators have been extensively investigated for their functional roles in PSC behaviors, including differentiation and subsequent tissue morphogenesis. The influence of biophysical cues and their subsequent cellular mechanotransduction, however, is not well understood[48, 78-81]. Specifically, investigations in the mechano-regulation of epigenetics that have been shown to play key roles in mammalian development and lineage specification, are only beginning to scratch surfaces, and

there is still a lack of knowledge on the potential mechanisms linking mechanotransduction and epigenetic regulation to determine stem cell fate[82]. Among various types of epigenetic regulation, DNA histone modification by methylation and acetylation, is an important process that has been shown to regulate PSC proliferation and germ layer differentiation through the activation or repression of gene expression related to stem cell fate[83, 84]. However, very limited number of studies have focused on elucidating how changes in cellular physical microenvironment or mechano-regulation affects PSC differentiation through the regulation of DNA histone modifications.

In this regard, this work aimed to utilize a 3D iPSC colony structure with diverse local mechanical microenvironment to unravel how mechanotransduction signaling mechanism intersects epigenetic regulation to control the iPSC differentiation at the early stages of development. Based on our previous study that showed the substrate stiffness-dependent iPSC colony formation, we investigated how such colony morphology, determining cell-cell and cell-substrate mechanical interactions, subsequently affect stem cell differentiation. Interestingly, heterogeneous differentiation within 3D iPSC colonies was observed when the cells were given freedom to differentiate toward all three germ layer lineages by BMP4 stimulation. RhoA/ROCK is one of the major components in the mechanotransduction pathways and regulates cytoskeletal organization in response to cell-cell and/or cell-substrate interactions[68, 71]. Our data show that the activity of RhoA is highly localized to the area of high tension, i.e., the

outermost layer of the 3D hemispherical colony, developing actomyosin cables. The inhibition of RhoA/ROCK signaling abolished the formation of the 3D structure, confirming the significance of substrate stiffness-mediated mechanotransduction in the formation of iPSC colonies. More significantly, we show that such heterogeneous mechanical microenvironment of individual cells within the colony regulates subsequent differentiation of iPSCs toward mesendodermal or ectodermal lineage.

Within the 2D islet culture of iPSCs, cells typically experience different mechanical environments depending on where they are located, these physical aspects have been shown to significantly affect signal transduction from the center to the edge of the 2D islets, resulting in location-dependent cellular behaviors[54, 85, 86]. Consistent with these studies, we found that iPSCs grew within a single 3D colony exhibit different RhoA/ROCK activity in a spatially dependent pattern in the radial direction, which leads to highly organized cytoskeleton structure, including the localized α-tubulin expression as well as the strong actin-myosin interactions at the outer layers of the 3D iPSC colonies. More interestingly, we revealed that the activity of histone modifications, H3K4me3 and H3K27ac showed similar patterned expression, also localized to the outer layers of the 3D colony and it is controlled by the YAP. YAP is an important transcription factor that responds to both physical and chemical environmental cues within the cells and has been shown to regulate histone modification[58]. Studies have shown that forces generated by cytoskeleton interactions can stretch nuclear pores to facilitate the

nuclear translocation of YAP[87]. This leads us to investigate whether RhoA/ROCK signaling is involved in regulating the YAP activity in the 3D iPSC colonies since we showed a close relationship between RhoA activity and cytoskeleton organization. The results demonstrate that RhoA/ROCK is required for the activation of YAP, suggesting that YAP acts as a mediator between mechanotransduction signaling and epigenetic regulation. Therefore, this work showed for the first time, to the best of our knowledge that heterogeneous mechanical microenvironment leads to differential responses of cellular mechanotransduction, resulting in spatially organized epigenetic activities and subsequent differentiation in 3D iPSC colonies. The elliptical iPSC colonies were engineered to further confirm the Rho/ROCK-YAP-epigenetic regulator signaling axis for the regulation of iPSC differentiation. The results from the elliptical colonies demonstrate that the heterogeneity of the physical environment causes spatially organized germ layer differentiation of iPSCs through a series of mechanotransduction pathway, including the activation of Rho/ROCK signaling, nuclear translocation of YAP transcription factor, and activation of histone modifications.

2.6 - Conclusion

In summary, the presented study demonstrates the significant role of mechanical microenvironment in determining the fate decision of PSCs and the potential of mechanically engineering a desired differentiation pattern. The system

may allow various investigations in the actions of mechanisms on biomechanically induced congenital defect formation during development. Further studies should involve exploring detailed mechanisms of how histone modifications affect iPSC early lineage differentiation. Moreover, the investigation of epigenetic regulations in response of cellular mechanotransduction behavior in our study limited to histone modifications while the relationship between DNA methylation, another important type of epigenetic regulations, and mechanical signalings remain unknown. Therefore, more studies need to be conducted to explore the effect of mechanotransduction on a broader aspect of the epigenetic regulations.

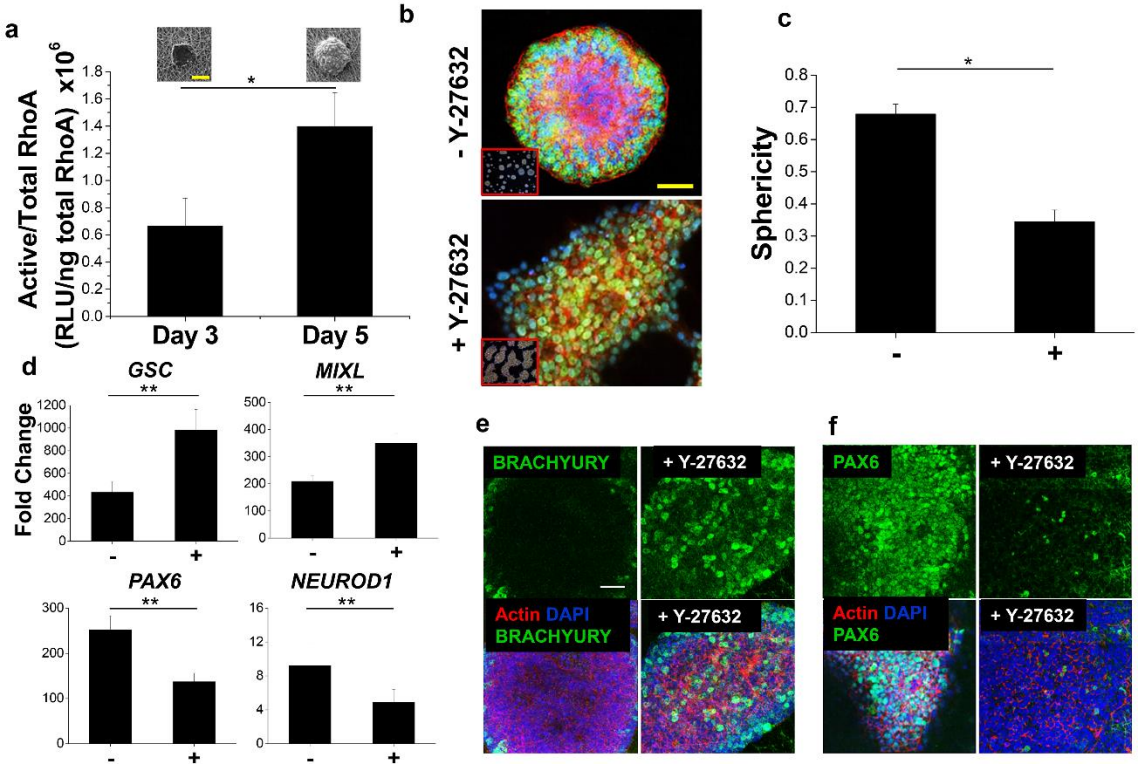

Figure 2.1. The colony morphology of iPSCs is regulated by the RhoA/ROCK signaling and affect subsequent directed differentiation. (a) iPSCs cultured on PCL scaffolds for 5 days resulted in 3D colony formation, exhibited significantly greater RhoA activity as compared to that of iPSCs cultured for 3 days on the same substrate. (scale bar=50μm, n=5, * denotes $p < 0.05$). (b) Fluorescence images showing morphological change of iPSC colonies cultured without (top) or with (bottom) the application of ROCK inhibitor (Y-27632). iPSCs cultured under all conditions-maintained expression of pluripotency marker NANOG (green: NANOG, red: ACTIN, blue: DAPI, scale bar=20 μm). (c) Quantification of colony sphericity without or with the application of Y-27632 (* denotes $p < 0.05$). (d) Gene expression levels of mesendodermal markers *GSC* and *MIXL*, and ectodermal markers *PAX6* and *NEUROD1* in iPSC colonies without or with the application of Y-27632 (** denotes $p < 0.01$). (e) Fluorescence images for the expression of mesendodermal marker Brachyury (T) in iPSC colonies without or with Y-27632 (white scale bar=10 μm). (f) Fluorescence images for the expression of ectodermal marker Pax6 in iPSC colonies without or with Y-27632.

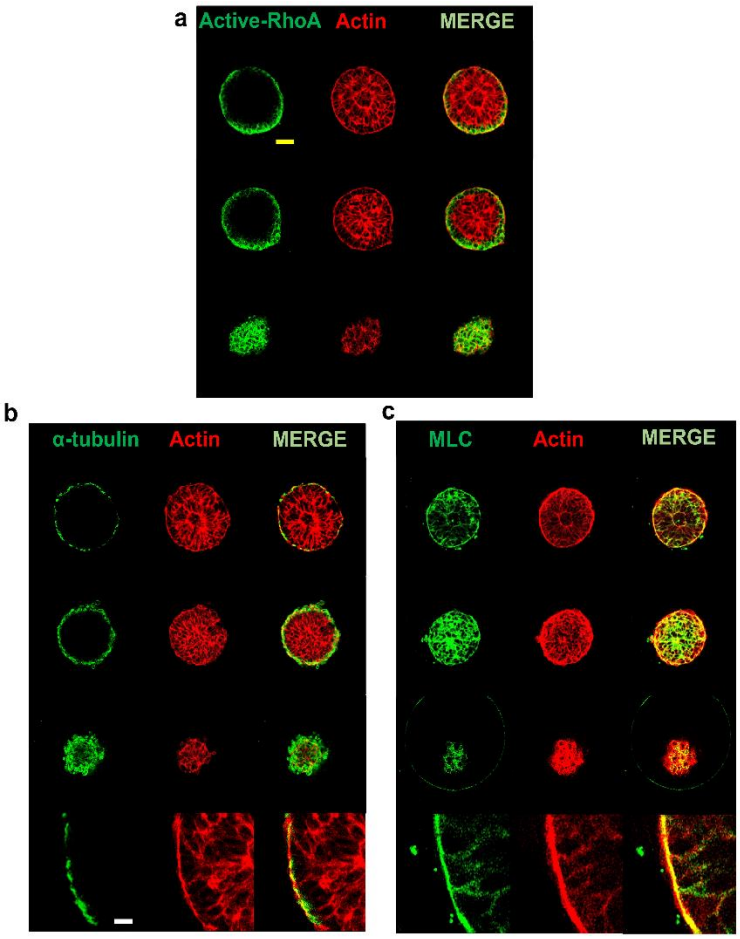

Figure 2.2. The hemispherical morphology of 3D iPSC colonies induces the localized expression of active RhoA and cytoskeleton components. (a) Representative confocal images of active-RhoA expression showing localized RhoA/ROCK activity in the outermost layers of the 3D iPSC colonies. (b, c) Representative confocal images of iPSCs colonies showing expression of (b) microtubule subunit α-tubulin (green) or (c) non-muscle myosin light chain (MLC) (green), actin filament (red), and nucleus (blue). Cells in the outermost layers of the 3D iPSC colonies show alternative patches of alpha-tubulin distribution and continued distribution of myosin light chain. Three representative cross-sectional images at the bottom, middle and top of the iPSC colonies are shown (yellow scale bar = 50 μm).

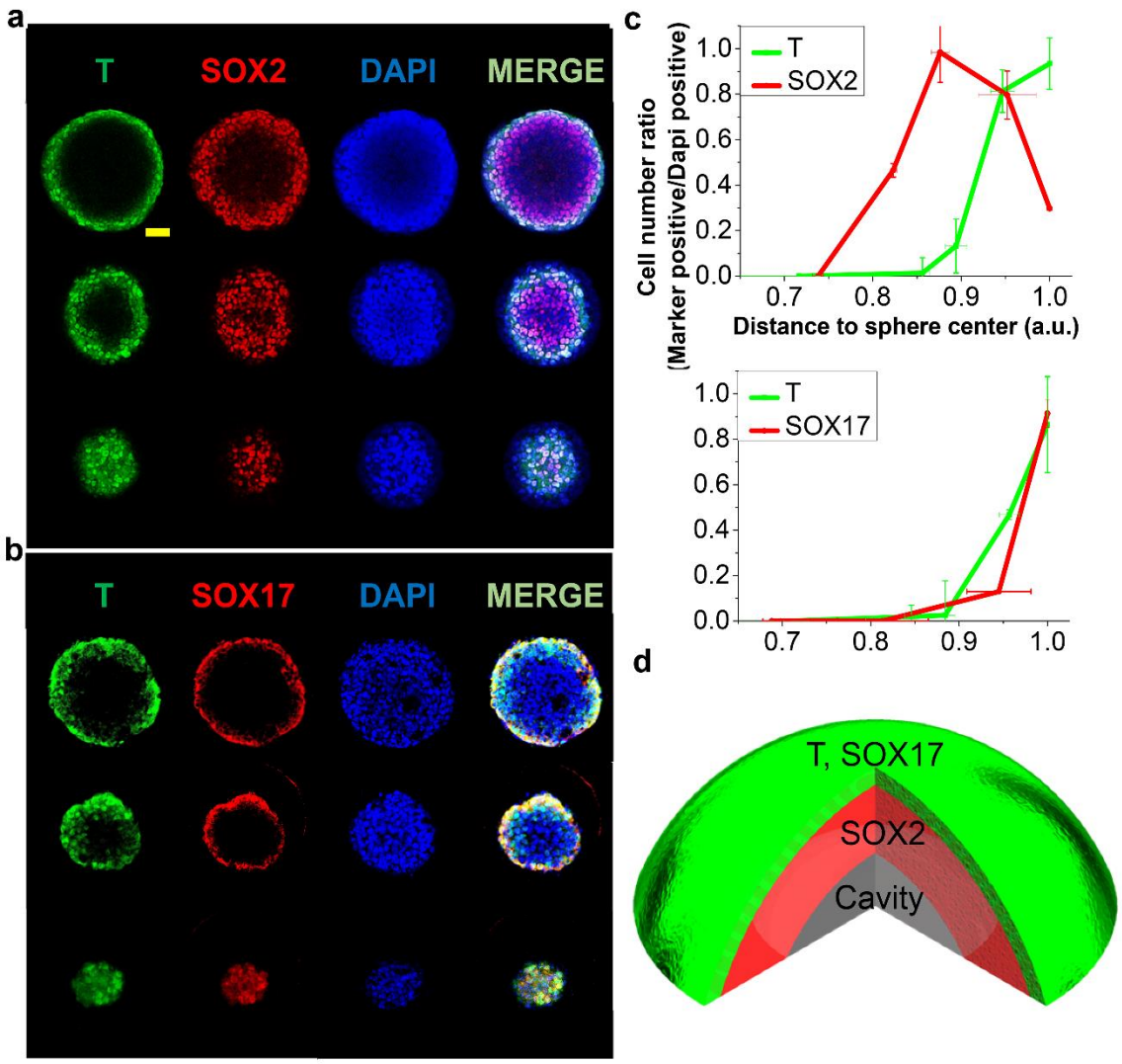

Figure 2.3. Organized germ layers are formed in 3D iPSC colonies under BMP4 induced spontaneous differentiation. (a, b) Confocal imaging of mesendodermal marker T and SOX17 expression shows that cells at the outermost layers of the 3D iPSC colonies preferentially differentiate to mesendodermal lineage while cells at the inner region of the colony tend to differentiate into ectodermal lineage, indicated by the expression of ectodermal marker SOX2. (c) Quantification of lineage mark expression showing the 3D radial distribution of mesendodermal and ectodermal differentiation. (d) Schematic of 3D radial distribution of cell lineages within the 3D cell colony under the BMP4 induction. Scale bar = 50 μm.

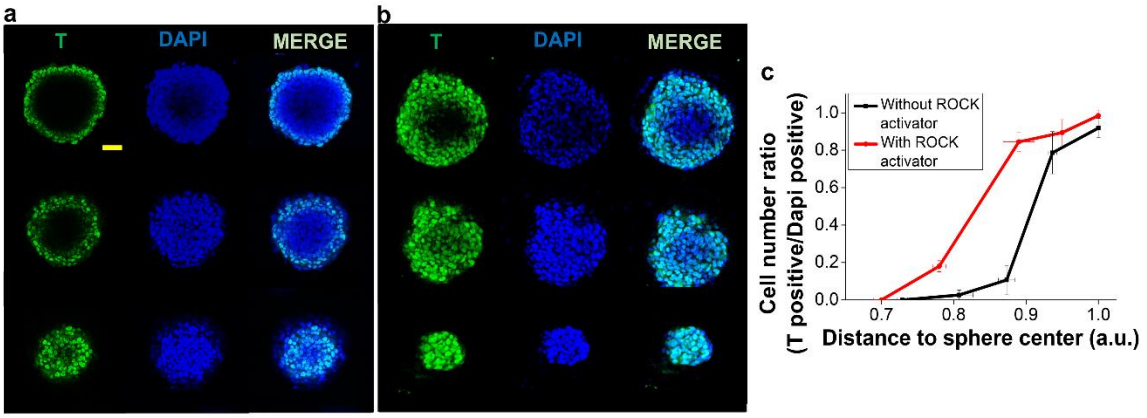

Figure 2.4. YAP signaling controls the activity of histone modification H3K4me3 and H3K27ac in the 3D iPSC colonies. (a-d) Representative confocal images showing the expression of YAP and H3K4me3 (a, b), or H3K27ac (c, d) in 3D iPSC colonies without (a, c) and with YAP inhibitor (5uM and 1-hour treatment) (b, d). (Scale bar = 50 μm.) (e-h) Quantification data showing the 3D radial distribution of YAP, H3K4me3-positive cells (e, f), and YAP, H3K27ac-positive cells (g, h) within the 3D iPSC colonies without (e, g) or with (f, h) the application of YAP inhibitor. Expression in cell nucleus was used for quantification (n = 3).

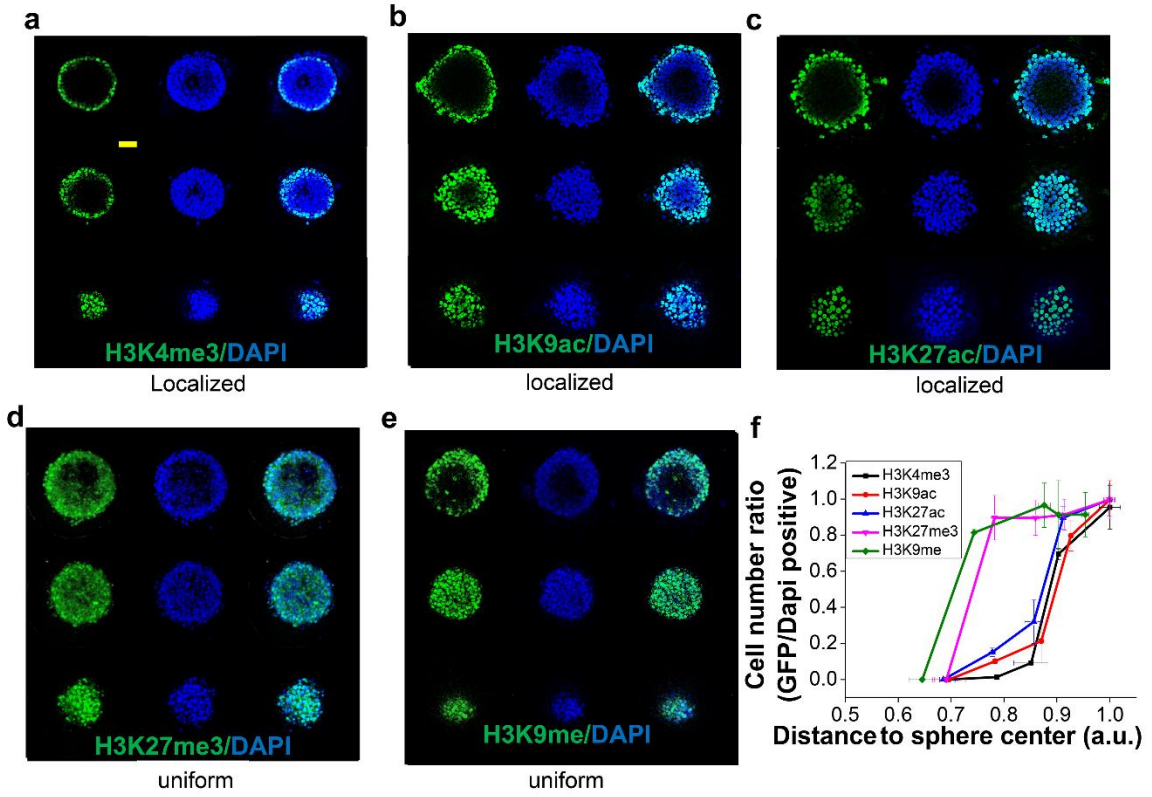

Figure 2.5. Epigenetic activities are localized within the 3D iPSC colonies. Confocal imaging shows localized histone modification within the 3D iPSC colonies, where the expression of activating histone modification including H3K4me3 (a), H3K9ac (b), and H3K27ac (c) is localized at the outermost layer of the colonies while repressive histone modification H3K27me3 (d), and H3K9me (e) show sparsely diffusive distribution throughout the 3D iPSC colonies. (Scale bar = 50 μm.) (f) Corresponding quantification of histone modification expression, showing the radial distribution of each epigenetic marker within the cell colonies (n = 3).

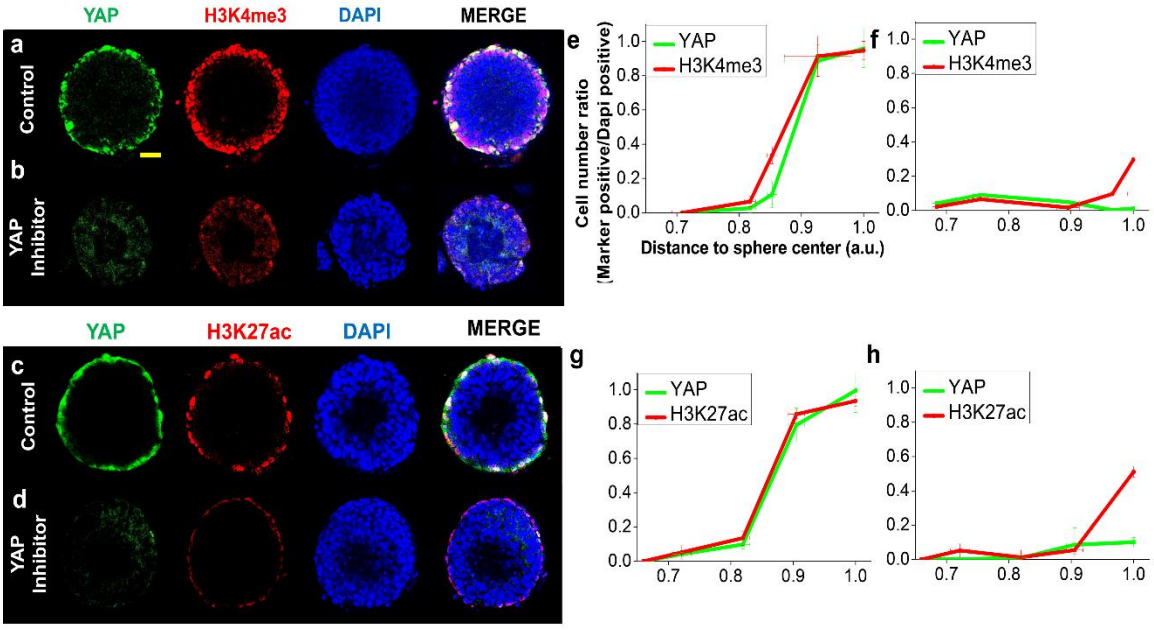

Figure 2.6. YAP signaling controls the activity of histone modification H3K4me3 and H3K27ac in the 3D iPSC colonies. (a-d) Representative confocal images showing the expression of YAP and H3K4me3 (a, b), or H3K27ac (c, d) in 3D iPSC colonies without (a, c) and with YAP inhibitor (5uM and 1-hour treatment) (b, d). (Scale bar = 50 μm.) (e-h) Quantification data showing the 3D radial distribution of YAP, H3K4me3-positive cells (e, f), and YAP, H3K27ac-positive cells (g, h) within the 3D iPSC colonies without (e, g) or with (f, h) the application of YAP inhibitor. Expression in cell nucleus was used for quantification (n = 3).

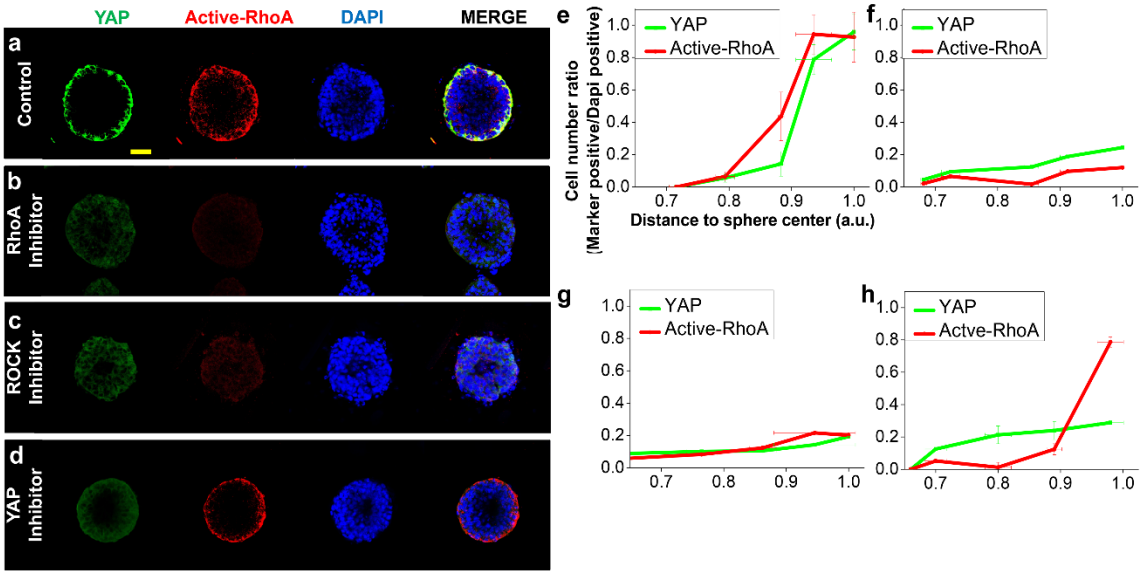

Figure 2.7. Rho/ROCK signaling regulates YAP activity. (a-d) Expression of YAP and active-RhoA under various conditions including RhoA inhibitor (b), ROCK inhibitor (c), and YAP inhibitor (d). iPSC colonies that were not exposed to any inhibitors were used as a control (a) (Scale bar = 50 μm). (e-h) Corresponding quantification data showing that the inhibition of Rho/ROCK signaling deteriorates YAP expression in the outermost layer of the colonies while YAP inhibition does not affect RhoA activity. (e) no inhibitor, (f) RhoA inhibitor, (g) ROCK inhibitor, and (h) YAP inhibitor. Markers that are expressed in cell nucleus were used for quantification (n = 3).

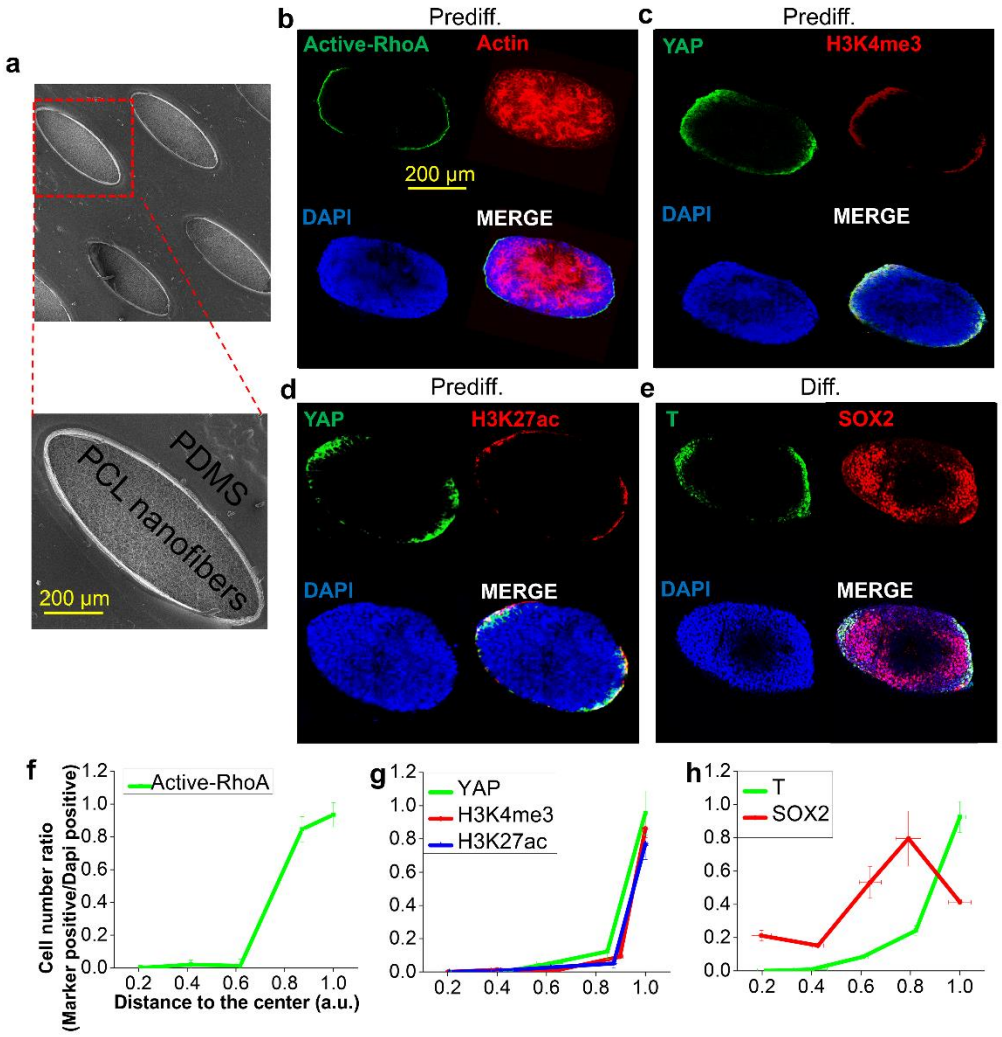

Figure 2.8. Rho/ROCK-YAP signaling axis regulates epigenetic modification of the cells in 3D iPSC colony and their subsequent differentiation. (a) SEM images showing the elliptical morphology of PDMS microwells attached to electrospun PCL nanofibers to physically control the morphology of 3D iPSC colonies. (b-e) Localized expression of various mechano-sensitive, epigenetic or differentiation markers including (b) active-RhoA and actin, (c) YAP and H3K4me3, (d) YAP and H3K27ac, and (e) T and SOX2. Mechano-sensitive markers (active RhoA and YAP) and epigenetic markers (H3K4me3 and H3K27ac) were examined after 5 days of preculture while differentiation markers (T and SOX2) were observed in the iPSC colonies which were subjected to subsequent BMP4 stimulation for 36 hours. (f-h) Corresponding quantification showing the localized expression of various markers in the longest axis within the elliptical cell colonies (n = 3).

CHAPTER 3. A MAGNETO-RESPONSIVE HYDROGEL SYSTEM FOR THE DYNAMIC MECHANO-MODULATION OF STEM CELL NICHE

3.1 - Abstract

The physical microenvironment of cells isn't constant, and their dynamic behavior is very difficult to capture *in vitro*. In this paper, a versatile and highly adaptive magneto-responsive hydrogel composed of magnetically sensitive nanorods and a stress-responsive polymeric matrix is demonstrated. Here we employ microengineered hydrogels with varying intensities of magnetic fields as well as altering the magnetic field polarity to induce hydrogel stiffening. The nanorod alignment after applications of low intensity magnetic fields using same magnetic field polarities as nanorod alignment, induces strain towards the polymeric network, resulting in stiffening (over 10-fold) at low nanorod (20 μg (nanorods)/mL (GelMA) solution) concentrations. Moreover, the stiffening mechanism can yield a fast and reversible response under a magnetic field. In this paper, we quantitively analyze the forces generated by the nanorods and examine their effects on induced pluripotent stem cell (iPSC) behavior and differentiation. This paper demonstrates the merit in utilizing an extrinsic magnetic field to stiffen the stem cell niche and can provide a platform to promote differentiation towards specific lineages. These results exemplify the versatility of our magneto-responsive hydrogel that can cater to 3D cell substrates and provides a platform to examine cellular behavior under dynamic mechano-modulation.

3.2. – Introduction

Over the past decade, the clinical potential of patient specific cell therapy has been substantially enhanced through the safe derivation and utilization of induced pluripotent stem cells (iPSCs)[88]. Human iPSCs not only offer the potential of personalized regenerative medicine but they also provide a cell/tissue platform to investigate human diseases without encountering ethical barriers or improperly using genetically mismatching animal-derived cells[89]. Among many factors, it is being more realized that the physical microenvironments of the cells significantly affect their differentiation and subsequent tissue development. Specifically, it has been demonstrated in various studies of embryonic development that mechanical cues drive stem cell differentiation toward specific lineages[5]. For example, immobilization of chick embryos using neuromuscular blocking agents results in a malformation of the skeletal system in the absence of dynamic mechanical stimulation from muscle contractions[90]. The compromised skeletal growth, in turn, leads to a decrease in muscle mass due to the lack of dynamic muscle contractions and a reduction of muscle force[91], demonstrating the significance of dynamic mechanical stimulation for the development of musculoskeletal system. Furthermore, studies have shown the involvement of biomechanical factors on the morphogenesis of various tissues such as cartilage, bone, and even the heart [92-94]. Such in vivo stem cell niches are mechanically dynamic microenvironments that are continuously evolved to balance cellular activities for tissue morphogenesis and homeostasis[95]. Therefore, extracellular matrix (ECM) modeling/remodeling is

integral in reciprocally modulating stem cell behaviors[95, 96]. In this case, it's important to be able to recapitulate these dynamic physical niches the cells experience.

In order to recapitulate the physical niches for desired stem cell behaviors, various types of scaffolds have been utilized to promote stem cell differentiation towards specific lineages/phenotypes[25]. Among numerous platforms, hydrogel systems including cell-derived Matrigel/Geltrex, tissue-derived collagen, hybrid gelatin methacrylate (GelMA), and synthetic polymeric scaffolds have been widely utilized due to their physicochemical similarities to the 3D microenvironments of in vivo ECMs. However, their static nature falls short in mimicking the dynamic stem cell microenvironments, especially the continuously evolving mechanical microenvironment, that guide tissue morphogenesis. Two major approaches to recapitulate the dynamic mechanical niche of cells in hydrogel systems involve: one utilizing the in-situ control over crosslinking density to control hydrogel stiffness. For example, Stowers et al. developed a reversibly tunable alginate hydrogel that relies on calcium concentration to improve the crosslinking efficiency, allowing for tuning of hydrogel stiffness[97]. A shortfall of this approach includes a small dynamic range of stiffness as well as a slower stiffening rate. The other approach utilizes exogeneous applied stimuli to control hydrogel stiffness such as temperature or a magnetic field. Hackelbusch et al. developed a thermo-tunable elastic hydrogel which enables reversible tuning of mechanical elasticity through the adjustment of temperature[98]. This method, however, is not suitable for

biological systems due to the temperature sensitivity of cells and tissues. On the other hand, magnetic fields in combination with magnetic nanoparticles (MNPs) embedded within the hydrogel has shown to be a possibility in dynamically controlling the mechanical microenvironment of cells while maintaining the proper conditions for cell viability. In this application, MNPs are used as a mediator converting the applied magnetic fields to the change of hydrogel stiffness by the motion of the particles, straining the polymeric network of the hydrogel[41]. Recently, Yan et al. developed a magnetic nanocomposite hydrogel with tunable stiffness utilizing the activation of the magnetic nanoparticles under a magnetic field, where the cells cultured on the hydrogel experienced and responded to the magnetic field-dependent stiffness change of the hydrogel[99]. One shortcoming of this approach is the efficiency of magnetic energy-to-hydrogel stiffness change in that a high intensity of magnetic field is required to obtain a relatively low range of stiffness change as several studies reported physiological and growth abnormalities of the cells cultured under strong magnetic fields[100]. Furthermore, the reversibility of the system is questionable as the application of magnetic fields resulted in a permanent deformation of the composite hydrogel.

In this study, a magneto-responsive hybrid hydrogel was synthesized by incorporating Fe_3O_4@SiO_2 magnetic nanorods (MNRs) within GelMA hydrogel, where the stiffness of hydrogel can be dynamically and reversibly modulated by the application of relatively low magnetic fields. Furthermore, a four electromagnet setup has been developed to simultaneously control the polarity and magnitudes

of the applied magnetic fields in real time allowing for the complete control over heterogeneous stiffness mapping (**Figure 3.1a**). We demonstrate that the application of magnetic fields predictably controls the local stiffness of the hydrogel, likely due to MNR rearrangement, straining the polymeric network of the hydrogel (**Figure 3.1b**). In addition, we show that pre-aligning of MNRs prior to hydrogel cross-linking further enhances the dynamic range of the stiffness change. Such control of the hydrogel stiffness significantly affects iPSC differentiation via the modulation over the Rho-ROCK signaling pathway, demonstrating the potential of the magneto-responsive hydrogel system for guiding stem cell-based tissue morphogenesis.

3.3 – Materials and Methods

3.3.1 - Magnetic Fe_3O_4-SiO_2 Nanorod (MNR) synthesis

The FeOOH nanorods were synthesized using a hydrothermal method. Typically, 19.464 g Iron chloride ($FeCl_3$, Sigma) was dissolved in 200 mL of deionized (DI) water. The solution was placed in an oven at 98 °C for 24 h. The obtained FeOOH nanorods were washed three times and redispersed in 160 mL of DI water. For the SiO_2 encapsulation of the nanorods, FeOOH nanorods were first modified by polyacrylic acid (PAA, Sigma); 40 mL of PAA (0.1 M) was added to the above solution and stirred overnight. The samples were centrifuged and redispersed in 50 mL DI water. Silica coating on FeOOH was then achieved by injecting 40 µL of tetraethyl orthosilicate (TEOS, Sigma) into a mixture containing

20 mL of ethanol, 1.5 mL of DI water, 0.5 mL of above FeOOH solution, and 1 mL of ammonium hydroxide ($NH_3 \cdot H_2O$, Fisher). After sonication for 30 minutes, the FeOOH-SiO_2 was collected by centrifuge and washed with ethanol and DI water. MNRs were synthesized through the reduction of FeOOH-SiO_2 nanorods at high calcination temperature. Briefly, FeOOH-SiO_2 nanorods were dried in crucibles and placed in a tubular furnace. The reduction occurred at 360 °C for 2 hours. After cooling down to room temperature, the prepared MNRs were washed with DI water three times.

3.3.2 – GelMA Synthesis

For the hydrogel preparation, 4 g of type A porcine skin gelatin was dissolved in 40 mL Dulbecco's phosphate buffered saline (DPBS; GIBCO) at 60 °C and stirred until fully dissolved. 3 mL of methacrylic anhydride (Sigma) was then added, at a rate of 0.5 mL/min, to the gelatin solution under stirring conditions at 50°C and the mixture was allowed to react for 1hr. The reaction was terminated by adding 120 mL DPBS and the mixture was then dialyzed for 5 days to remove any unreacted methacrylic anhydride or byproduct acrylic acid. The polymer solution was lyophilized for 7 days. The GelMA precursor solution was prepared by dissolving certain amount of GelMA into the DPBS, having 0.05% of photoinitiator lithium phenyl-2,4,6-trimethylbenzoylphosphinate (LAP).

3.3.3 – MNR alignment and encapsulation

To incorporate MNR into the GelMA hydrogel, various concentrations of MNRs in GelMA precursor were used. 1 mL of 7.5 wt% GelMA precursor was placed into a 1.5 mL microcentrifuge tube while mixing with 3, 10, 20, or 30 μg of MNRs. The GelMA/MNR precursor solution was sonicated at 37°C for 1 min to prevent MNR aggregation. To align the MNRs within the GelMA precursor, 40 μL of the GelMA/MNR precursor solution was pipetted into a PDMS mold, having an empty hole of 6 mm in diameter and 1 mm in depth, and was then placed at the center of four 12 V DC electromagnets (McMASTER-CARR). 7.5 mT of the magnetic field, generated by the four electromagnets with north polar facing inwards (same polarity), was applied to the GelMA/MNR precursor solution for 5 minutes. The precursor was then crosslinked using UV light for 90 s. The GelMA precursor without aligned MNRs was also crosslinked as a control group. Magnetic field intensities were measured using a Gauss meter (HT20, Resolution: 1 mT) on the surface of the north pole.

3.3.4 – Mechanical characterization of MNR embedded hydrogel under magnetic field

The Reduced Young's Modulus of the randomly oriented or aligned MNR hydrogel with different MNR concentrations under various magnitudes/polarities of the applied magnetic fields, was measured using a MFP-3D AFM (Asylum Research, Santa Barbara, CA). To apply the external magnetic fields while

measuring the reduced Young's Modulus, the hydrogel samples were placed at the center of the four electromagnets as shown in **Figure 3.1**.

3.3.5 – iPSC culture in MNR-incorporated hydrogel

A well characterized human iPSC cell line, derived from BJ-2522 human neonatal foreskin fibroblast cells transfected with OCT4, SOX2, and KLF4[101, 102], was maintained on Geltrex-coated tissue culture polystyrene plates (TCPS) in mTeSR™ 1 medium (Stemcell Technologies, Vancouver, Canada) in a humidified incubator at 37 °C and 5% CO_2 prior to their inoculation into the MNR-incorporated hydrogel.

The cells were detached from the culture plates using Accutase (Fisher) and mixed with the hydrogel precursor solution of 15 wt% of GelMA precursor to achieve a 2 million cells per mL. 40 µL of cell/GelMA precursor solution was mixed with 0.8 µg of MNRs (20 µg/mL) and pipetted into the previously mentioned PDMS mold in a petri-dish in which the final GelMA concentration was 7.5 wt%. The precursor was then photocrosslinked for 20 s under UV light exposure either with or without pre-aligning the NMRs as previously described. 10 µM of Y-27632 (Sigma) was added during the first 24 hours of culture duration after crosslinking to enhance the cell viability.

After 5 days of pre-culture period, the cell/GelMA complex having non-aligned or aligned MNRs (20 µg/mL of GelMA) was exposed to 4.5 mT of magnetic field for 1 hour before being fixed with 4% paraformaldehyde (PFA, Fisher). The

cells encapsulated within the hydrogel without any MNR was also fixed and used as a control. To examine iPSC differentiation behavior within anisotropic stiffness hydrogel, iPSCs were pre-cultured for 5 days and then treated with BMP4 (40 ng mL^{-1}) for 36 hours while applying a magnetic field of 4.5 mT (same polarity as pre-alignment) for the entire duration of the 36 hour differentiation to induce simultaneous germ layer differentiation. Differentiated 3D iPSC colonies were fixed using 4% paraformaldehyde.

3.3.6 – iPSC viability assessment

Cell viability for cells encapsulated in 7.5 wt% GelMA and the hydrogel with either randomly oriented or aligned MNRs were assessed through a live/dead cell assay (Invitrogen). Cells were cultured for 3, 5,and 7 days before the viability assay. The cells were stained with 0.5 µl/mL of calcein AM and 2 µl/mL of ethidium homodimer-1 (EthD-1) in DPBS for 5 mins at room temperature. Fluorescent image acquisition was carried out using a Nikon-Eclipse TI microscope (). Viable cells appear as green while dead cells as red. Cell viability % was evaluated using ImageJ.

3.3.7 – Immunofluorescence imaging

Samples were immuno-stained following a standard immunofluorescence staining protocol. Briefly, the fixed samples were permeabilized by 0.1% Triton-X in a phosphate buffered saline (PBS) followed by blocking of non-specific binding

sites with 1% bovine serum albumin (BSA) in PBS. The following antibodies were utilized for the detection of specific protein expression: rabbit anti-YAP (Cell Signaling), mouse anti-Active RhoA-GTP (NewEast Biosciences), goat anti-BRACHYURY (R&D Systems), rabbit anti-SOX2 (Cell Signaling) and appropriate secondary antibodies. The samples were then counter-stained with 4′,6-diamidino-2-phenylindole **(**DAPI, Sigma) to visualize the nuclei. The confocal imaging was performed using a Zeiss 880 microscope.

3.3.9 – Image analysis

Imaris 7.1.1 (Bitplane) was used to analyze the colony morphology of iPSCs from confocal imaging to measure the sphericity (*i.e.*, ratio of the surface area of a sphere to the surface area of the object).

3.3.10 – Statistical analysis

All experiments were conducted with a minimum of triplicate biological samples and data is represented as mean ± standard deviation (SD). Comparison of groups for statistical significance was determined using SPSS 15 software with one-way ANOVA analysis with Tukey's posthoc.

3.4 – Results

The working principle of our proposed strategy to utilize magneto-responsive hydrogel system for the mechano-modulation of stem cell niche is

based on the straining of hydrogel polymer network by the re-arrangement of MNPs within the hydrogel under the applied magnetic fields. Therefore, the shape of the MNPs is an integral factor determining the efficiency of magnetic field-induced hydrogel stiffening. To examine the effects of the shape factor, strain maps of crosslinked hydrogel networks incorporated with MNPs having either a rod (MNR) or spherical (MNS) shape with the same volume, in response to an applied magnetic field were determined by COMSOL modeling (**Figure 3.2a**). With the magnetic field acting along the x-axis, the MNRs demonstrated to produce a greater stiffness gradient, resulting in a greater stiffness change in its surroundings, with its average stiffness nearly 7 times greater than that of the MNSs. Based on these simulation results, MNRs were employed in the subsequent experiments to induce the maximal stiffness change throughout the hydrogel with a minimal applied magnetic field.

In order to obtain an evenly distributed magnetic field, the optimal configuration/placement of the electromagnets was determined by COMSOL modeling. The same polarity on each electromagnet generated the magnetic field gradients to evenly align in the center of those orthogonally positioned electromagnets, where the MNR-incorporated hydrogel will be placed (**Figure 3.3a**). Based on the series of COMSOL simulation, a relatively uniform distribution of MNRs was obtained when approximately 7.5 mT of the magnetic field was applied for 5 mins (**Figure 3.3b**).

Hydrogel samples with various amounts of the pre-aligned MNRs were photo-crosslinked by an exposure to UV and then further subjected to various magnitudes of the applied magnetic fields to investigate the MNR loading-dependent dynamic stiffness range. Furthermore, the effect of the applied magnetic polarity, either the same or opposite to the magnetic field applied during the pre-alignment was investigated. As expected, the dynamic range of stiffness change increased as the MNR loading increased when the average stiffness was calculated from AFM measurements at 9 different areas per condition (**Figure 3.4**). Specifically, 3 μg/mL condition did not exhibit an appreciable change in stiffness under any applied magnetic fields. However, the increase in the MNR loading not only increased the dynamic stiffness range but also enhanced response time required to reach to the stable stiffness earlier. Interestingly, the application of the opposite polarity to the magnetic field applied during the pre-aligning induced less stiffness changes in all conditions. These results demonstrate the magneto-responsive hydrogel system delivers tightly controlled stiffness changes from 7 kPa up to nearly 100 kPa, significantly superior to other magneto-responsive systems[4, 99]. Based on previous studies from ours as well as others, which determined the stem cell-relevant stiffness range[103-105] , the 20 μg/mL condition was used in the rest of this study.

To demonstrate the effect of MNR orientation, the stiffness changes of hydrogel with pre-aligned MNRs were compared to that of hydrogel with randomly oriented MNRs under various magnitudes of magnetic fields (**Figure 3.5**). The

application of 7.5 mT with all electromagnets set to the same polarity for 5 minutes prior to UV crosslinking for the MNR loading of 20 μg/mL resulted in the MNR alignment as shown in **Figure 3.5a**. Subsequent application of magnetic fields with the same polarity to the pre-alignment induced the stiffness change from 13 kPa up to 61 kPa. In contrast, the hydrogel with randomly oriented MNRs exhibited an inferior dynamic stiffness range from 13 kPa to around 20 kPa. These inferior results are a result of the randomly oriented magnetic ends of the nanorods being fixed to their current positions restricting them from rotating towards the opposing magnetic field polarity which results in an inferior stiffness range. These results demonstrate the enhancement of dynamic stiffness change by pre-aligning MNRs, more than 300% as compared to randomly oriented MNRs.

The detailed effects of magnitude and polarity of the applied magnetic fields on the hydrogel stiffness were determined by measuring the stiffness changes in the local area of system (**Figure 3.6**). The samples were subjected to the stepwise magnitude and polarity changes of the applied magnetic fields after pre-aligning MNRs and crosslinking the hydrogel. As shown earlier, the magnitude of the applied magnetic field was the pre-dominant factor determining the stiffness of the hydrogel. The polarity of the applied magnetic field, however, also differentially influenced the stiffness change, where the same polarity to the magnetic field used for pre-aligning MNRs induced greater stiffness changes as compared to those from the opposite polarity. As expected from the distribution of MNRs within the hydrogel, the stiffness change showed location-dependency; a similar, higher

increase in the reduced Young's modulus was observed in the regions with the MNRs oriented toward the magnetic field (*i.e.*, Points 2-5; approximately an average of 10 kPa-70 kPa when 4.5 mT of the same polarity was applied) whereas the center of the hydrogel, Point 1, experienced less stiffness changes from approximately 10 kPa to 40 kPa under the same applied magnetic fields. These results indicate that the stiffness change at a specific location within the hydrogel can be predicted by the local alignment of MNRs. Furthermore, the magneto-responsive hydrogel system was subjected to a repeated cycle of the step-wise magnetic field changes. The system demonstrated its superb repeatability over various stimulation regimens, showing its reversible capability, being able to stiffen and soften the hydrogel under changing magnetic polarities and field intensities (**Figure 3.6g**).

To further demonstrate the versatility of the hydrogel system to present anisotropic, yet predictable stiffness changes in its local areas, three different magnetic field configurations were used at a magnitude of 4.5 mT, in which nine different points in the hydrogel were measured (**Figure 3.7a-c**). The same polarity configuration, Configuration 1, induced the greatest change in stiffness, where the sides nearest to the magnetic field (Points 2-5), 50-70 kPa, experienced greater stiffness change than Point 1, middle region, of the hydrogel (~25 kPa) (**Figure 3.7d**). The diagonal corners of the electromagnets (Point 6-9) experienced a similar increase in stiffness to those in Points 2-5. In contrast, the second configuration, where the hydrogel was exposed to two different polarities, the top

and bottom experiencing the same polarity while the right and left regions experience the oppose polarity at 4.5 mT, generated an anisotropic stiffness change (**Figure 3.7b**); the sides of the same polarity (*i.e.*, Points 2 and 5) experienced a substantially increased stiffness change, approximately at 50 kPa while the regions subjected to the opposite polarity (*i.e.*, Points 3 and 4) experienced only a slight stiffness increase, approximately at 20 kPa (**Figure 3.7e).** When the magnetic field polarity was switched, a similar pattern of stiffness change was observed, where the sides of magnetic fields with the same polarity to the pre-aligning magnetic field exhibited a greater stiffness change than those with the opposite polarity in a predictable manner (**Figure 3.7f)**. These results demonstrate the capability of the system to apply an anisotropic, local stiffness change in a predictable manner, enabling the application of the subjection of individual cells to various magnitudes of stiffness within a single cell culture.

For the application of the system for biological studies, the potential cytotoxicity of the GelMA hydrogel incorporated with MNRs was tested. Human iPSCs were inoculated in the hydrogel either with or without MNRs and their viability was determined using a live/dead cell assay for various culture durations (**Figure 3.8**). There was no statistically significant effect of MNRs as all conditions exhibiting high cell viability above 90%. The cells also formed spherical colonies with their size increasing over the 7-day culture duration.

To examine the effects of hydrogel stiffness control on stem cell behaviors, iPSCs were seeded into the hydrogel system and precultured for 5 days prior to

being subjected to the applied magnetic field. The application of magnetic field at 4.5 mT without the presence of MNRs (control) did not induce the expression of Active-RhoA and YAP, both of which are mechano-sensitive signaling mediators. (**Figure 3.9a**). In contrast, iPSCs that were seeded with randomly oriented nanorods and subjected to one hour of 4.5 mT after 5 days of pre-culture exhibited cytoplasmic localization of Active-RhoA on the outer regions of the colony, indicating RhoA activation, while YAP becomes localized in the nuclei in the cells near the outer regions of the colony (**Figure 3.9b**). Interestingly, the cells in the aligned MNR samples exhibited the greatest expression of active-RhoA with its cytoplasmic localization, as well as further activation of YAP. The quantification of the intensity of these mechano-sensitive molecules confirmed the enhanced cellular responses in the aligned MNR samples likely due to the greater stiffness changes (**Figure 3.9b**).

Based on the results demonstrating the system's capability to generate a heterogeneous stiffness field within the individual hydrogel when exposed to anisotropic magnetic fields (Figure 3.7), the local stiffness-dependent iPSC differentiation was investigated. Cells were inoculated into hydrogel with pre-aligned MNR and pre-cultured for 5 days before the application of anisotropic 4.5 mT magnetic field as shown in **Figure 3.7b**. Under anisotropic strain and simultaneous biochemical stimulation with BMP4, the morphology of cell colonies significantly changed depending on local hydrogel stiffness. As shown in the 3D reconstructed images, the cells formed a discoidal colony within the stiffer region

of the hydrogel while the colonies in the softer region maintained their spherical morphology (Figure 3.10). Interestingly, the migrating cells that are responsible for the colony morphology change in the stiffer region expressed Brachyury (T), a mesendodermal marker while Sox2, a ectodermal marker, was expressed in the cells localized in the center of the colonies in the stiffer region or the cells in the softer region of the hydrogel. The difference in the colony morphology was quantitatively assessed by measuring their sphericity, a degree of shape relative to the perfect sphere, through the 3D rendering of confocal images, showing the regional stiffness-dependent colony morphology under the same biochemical environment (**Figure 3.10c**). The impact of stiffness-dependent colony morphology on the differentiation of iPSCs was quantified by comparing the number of cells expressing mesendodermal or ectodermal marker, where the stiffer region promoted mesendodermal differentiation especially in the migrating cells from the colonies (**Figure 3.10d**).

3.5 - Discussion

In vivo, stem cells sense their niche and differentiate in accordance with their physicochemical microenvironment[106]. During the development, the ECM secreted from these differentiating cells and the forces from neighboring tissues dynamically alter their biomechanical environment, further stimulating the cells and guiding their tissue morphogenesis. To understand the role of mechanical factors on cellular behaviors, numerous studies have focused on statically controlling the

physical microenvironment by utilizing scaffolds of different stiffnesses[107, 108] or unidirectionally stiffening or softening hydrogels via time-dependent increase or decrease in cross-linking density[109, 110]. Although these systems provide excellent platforms to study mechanobiology they often fail to capture the dynamic nature of in vivo microenvironment especially during tissue morphogenesis. One approach to dynamically and reversibly control matrix stiffness utilizes the hydrogel with reversible mechanics by in-situ control over crosslinking density[111, 112]. This approach requires exogenous chemical[97] (e.g., Ca^{2+}) or physical (UV/NIR) stimuli to control the interaction among hydrogel polymer network, hence its stiffness, but such stimuli may also directly affect cells through Ca2+ signaling and heat shock proteins[113, 114]. Another approach utilizes the magneto-responsiveness of MNPs embedded within hydrogel[114-117]. However, these systems require substantial magnitudes of magnetic fields in the range of hundreds of mT, often causing heat generation issues when magnetic generators (e.g., electromagnet) are used to dynamically regulate magnetic fields.

To address the shortcoming of MNP-based systems requiring high magnetic fields for stiffness control, we utilized two separate yet collaborating approaches. The mechanism underlying the stiffening of the hydrogel lies within the microscopic movement of the MNPs, straining the polymeric fibers of the hydrogel in response to the magnetic stimuli. Instead of spherical MNPs (MNSs), we employed a rod shape of MNPs (MNRs); since MNRs have a clear polarity with respect to the length of the particle, changing the polarity of a magnetic field causes

MNRs to rotate in addition to their translational motion, exerting greater strains to the surroundings in comparison to MNSs as demonstrated in our numerical study. Kim et al. even demonstrated that MNRs can align longitudinally along electrospun polymeric fibers and are able to maximize forces generated under magnetic fields more efficiently in comparison to MNSs[118]. This magnetic anisotropy in MNRs allows alignment of the particles according to a magnetic field, providing an opportunity to maximize the magneto-responsiveness of the system; the pre-alignment of MNRs before hydrogel crosslinking resulted in nearly 200% increase in the stiffness change as compared to that of randomly oriented MNRs within the hydrogel, likely due to avoiding the cancelling effect of random orientation. The improvement in the magneto-responsiveness reduced the required magnetic field to two orders of magnitude, from hundreds of mT to several mT[4, 114, 115, 119]. The response time of the system is also significantly enhanced as the stiffness change was stabilized within minutes of magnetic field application as compared to hours required to reach the maximum stiffness change in other systems[99]. Furthermore, the dynamic range of stiffness change was also improved to cover the physiologically relevant range to direct diverse cellular responses.

The pre-alignment of MNRs also enables faster reversible change in stiffness and its anisotropic distribution within the same hydrogel in a predictable manner. As demonstrated in the disproportional stiffness change under different polarities, the movement of the MNRs within the hydrogel, hence straining of hydrogel polymeric network is influenced by the polarity as well as the magnitude

of the magnetic field. As shown in the response under a stepwise magnetic field stimulation, removal of the magnetic field does not result in the immediate recovery of the original hydrogel stiffness, likely due to the viscoelastic nature of the hydrogel. The application of magnetic field in the opposite polarity, however, can readily change the hydrogel stiffness to the original state. Based on the disproportional stiffness response under the different polarities of the applied magnetic fields, we also demonstrated the generation of variable stiffness field with the hydrogel by utilizing the anisotropic application of magnetic fields. The local stiffness of the hydrogel was precisely controlled where regions that were exposed to the same polarity to the pre-aligning magnetic field experienced the highest change in stiffness in comparison to regions under the opposing magnetic field polarity. This is due to the location, hence, magnetic field-dependent simultaneous attractive and repulsive forces from the MNRs to the surrounding hydrogel, which then result in anisotropic distribution of softer and stiffer regions. These results demonstrate the potential use of the magneto-responsive hydrogel for mechanobiology studies where the mechanical factor can be decoupled from other physicochemical factors by culturing the cells in the same biochemical conditions yet in the different local mechanical environment.

The feasibility of the system for mechanobiology study was demonstrated by investigating both a short-term cellular response and a long-term iPSC differentiation. Among various mechano-responsive signaling cascades, the Rho/ROCK signaling pathway has been shown to be vital in determining stem cell

fate[120]. The Rho/ROCK signaling drives cytoskeletal remodeling and regulates gene expression in response to the mechanical change in microenvironment (e.g., change in stiffness) leading to lineage specification[121]. iPSCs seeded in the hydrogel without MNRs or not subjected to magnetic fields did not exhibit Rho/ROCK and YAP signaling activation. In contrast, iPSCs that were seeded within the hydrogel with randomly oriented and aligned MNRs both exhibit Active-RhoA and YAP activation, however, the aligned MNR condition showed greater expression of these mechano-sensitive markers. Due to the dynamic stiffening, the Rho/ROCK signaling pathway was activated in which the actin myosin bundles reciprocated to compensate for the change in the physical microenvironment, hence leading to the activation of YAP. We also showed stiffness-dependent differentiation of iPSCs by applying anisotropic magnetic fields to create a gradient of stiffness field within the hydrogel. Colonies positioned in the stiffer regions exhibited the migration of T-positive cells, similar to that observed during embryo development. In contrast, colonies in the softer regions exhibited a more spherical morphology with greater Sox2 expression. Previous studies have shown how the mechano/physical niche can affect iPSC dimensionality and differentiation patterns, where higher expression of mesendodermal markers are observed in the iPSC colonies on stiffer scaffolds stress versus softer scaffolds that induce greater ectodermal differentiation[2]. These results demonstrate that our magneto-responsive hydrogel system with pre-aligned MNRs can produce a monolithic culture platform with a controlled gradient of hydrogel stiffness in 3D, providing a

means to subject cells to diverse mechanical microenvironment under the otherwise identical culture conditions.

3.6 – Conclusion

Overall, we report that the GelMA hybrid hydrogels incorporated with MNRs show a strong mechanical response to low intensity magnetic fields. Due to the nanorod's ferromagnetic properties, increasing magnetic field magnitude coupled with altering magnetic field polarity can enhance the dynamic range of reversible hydrogel stiffness. The pre-alignment of MNRs prior to hydrogel crosslinking not only further enhances the dynamic range but it also enables the generation of stiffness gradient in a location-specific manner. The feasibility of the system in mechanobiology studies is demonstrated from the activation of the mechano-sensitive Rho/ROCK and YAP signaling pathways, indicating that the magneto-responsive hydrogel can manipulate the physical niche of the stem cells by activating cytoskeletal remodeling. The exogeneous application of a magnetic field with the synergistic effects of MNR pre-alignment offers ease of use, mechanical environmental modulation, as well as dynamic control of the physical niche of stem cells to obtain local stiffness-dependent cellular responses within the same substrate. Collectively, these results demonstrate the versatility and reliability of the mechano-responsive hydrogel system as an excellent platform for studying mechanobiology of various cells/tissues for the discovery/development of potential therapeutics.

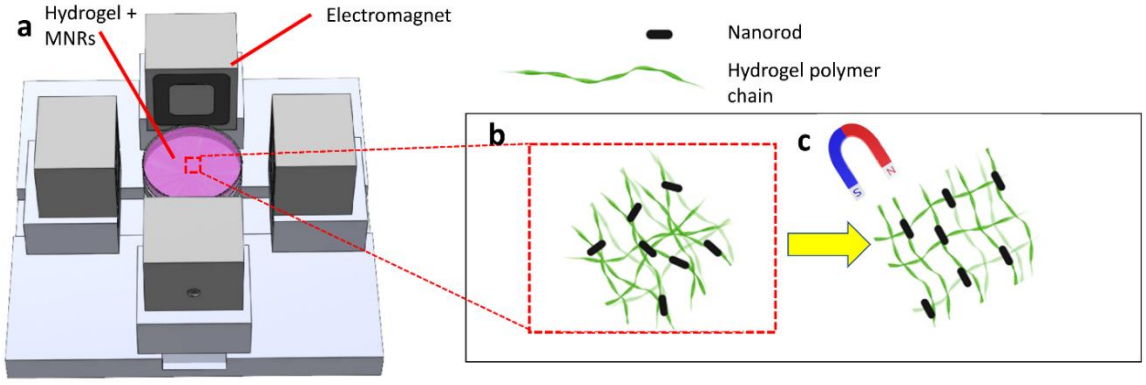

Figure 3.1. Schematic of a magneto-responsive hydrogel system for the dynamic mechano-modulation of stem cell niche, based on the stiffening of the hydrogel due to mechanical straining by magnetic nanorod (MNR) re-orientation under the applied magnetic fields. (a) Magnetic Fe_3O_4@SiO_2 nanorod-containing 7.5 wt. % Gelatin methacrylate (GelMA) hydrogel placed in the center of four electromagnets. (b) Randomly distributed MNRs in the hydrogel network. (c) Mechanical straining when exposed to magnetic fields (Graphics are not up to scale).

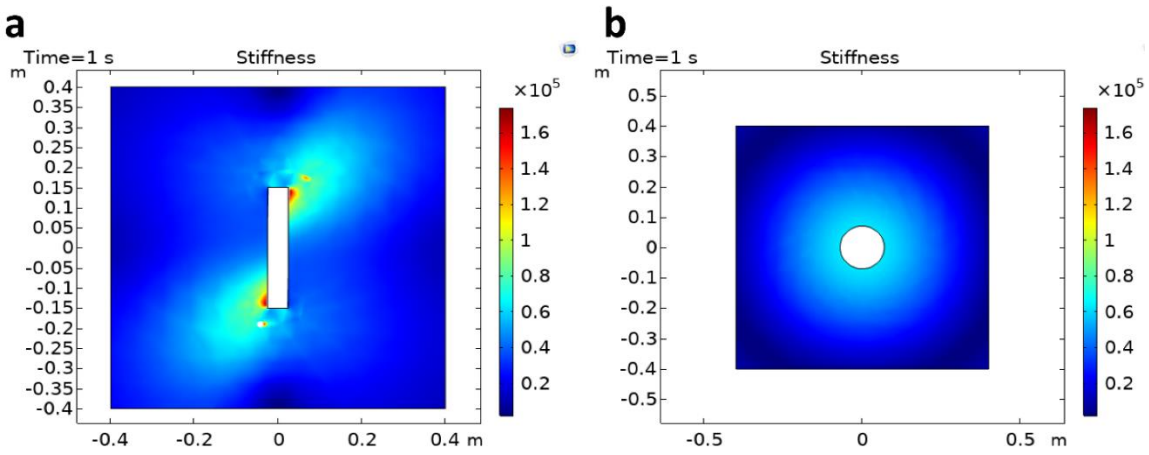

Figure 3.2. Computational modeling of magnetic particle shape-dependent hydrogel straining. COMSOL Multiphysics modeling showing the greater hydrogel straining under the applied magnetic fields, leading to the greater hydrogel stiffness changes with (a) magnetic nanorod as compared to those with (b) magnetic nanosphere.

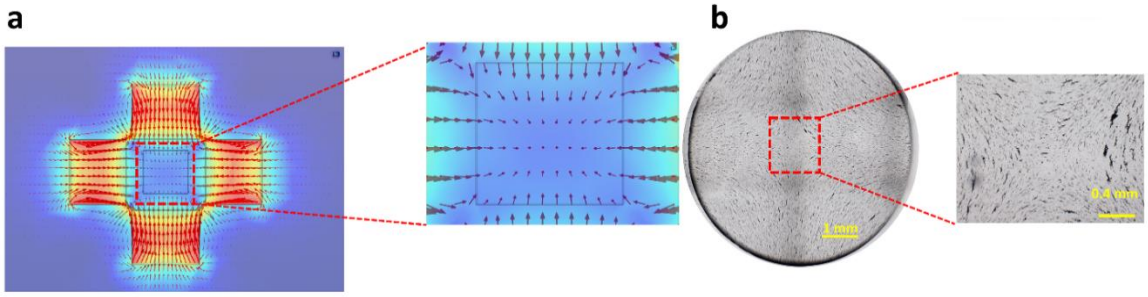

Figure 3.3. The alignment of magnetic nanorods (MNRs) under the applied magnetic fields by the electromagnets with the same polarity. (a) COMSOL modeling of magnetic field gradients and (b) MNR alignment within hydrogel after an exposure to magnetic fields at the magnitudes of 7.5 mT for 5 mins.

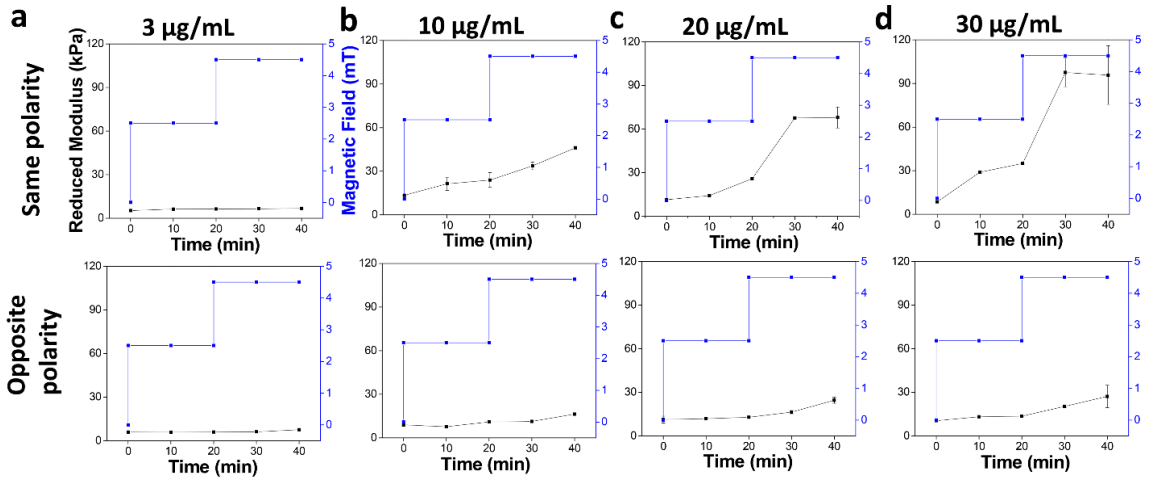

Figure 3.4. Stiffness change of hydrogel depending on the loading of pre-aligned magnetic nanorods (MNRs) and the polarity of the applied magnetic fields under various magnitudes of magnetic stimulation. Stiffness changes of hydrogel having (a) 3 µg/mL (GelMA), (b) 10 µg/mL, (c) 20 µg/mL, and (d) 30 µg/mL of MNRs subjected to the applied magnetic fields with various magnitudes and polarities. The stiffness was in situ measured by atomic force microscopy.

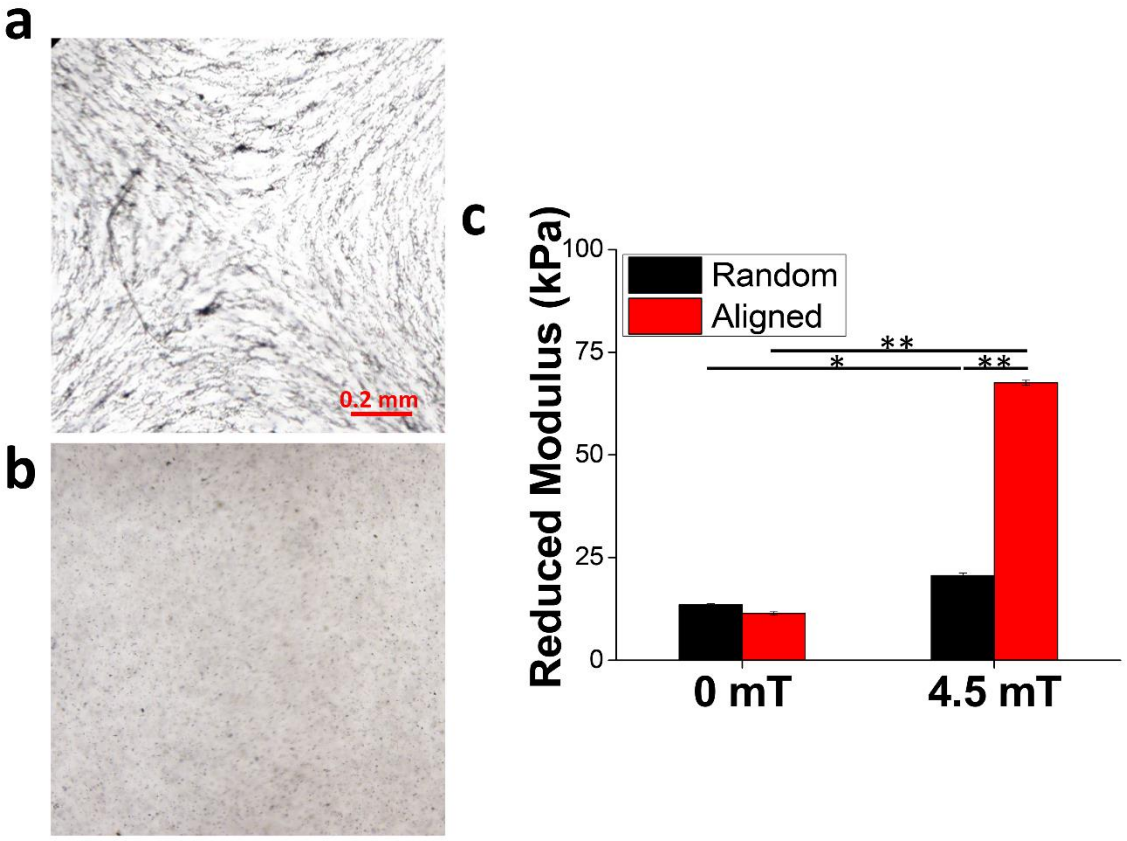

Figure 3.5. The effect of pre-aligned magnetic nanorods on the stiffness change of hydrogel. Images of hydrogel with (a) pre-aligned magnetic nanorods and (b) randomly oriented nanorods. (c) Reduced Young's modulus of GelMA hydrogel with randomly oriented or aligned nanorods under the magnetic application of 4.5 mT ($n = 5$, * and ** denote statistical significance of $p < 0.05$ and $p < 0.01$, respectively.).

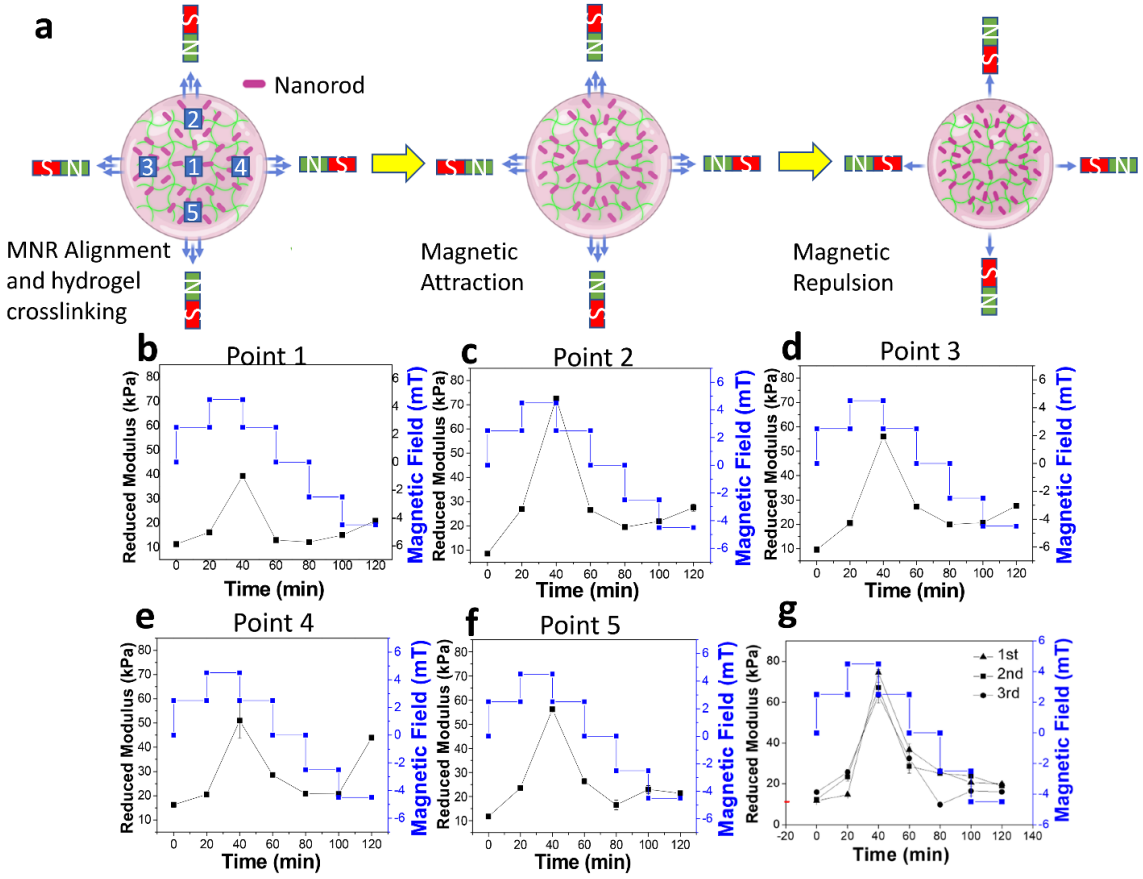

Figure 3.6. Local stiffness change of magnetic nanorod (MNR)-incorporated hydrogel under various magnitudes and polarity of the applied magnetic fields. (a) Schematic showing the procedure of MNR pre-alignment, stiffness measurements under the same polarity with the pre-aligning, followed by stiffness measurements under the opposite polarity. (b-f) Changes in the reduced Young's modulus at different locations of the hydrogel as shown in (a). (g) Reversibility and repeatability of stiffness control in the hydrogel incorporated with pre-aligned MNRs. At least nine stiffness measurements from various points around the hydrogel were used for the presented averages.

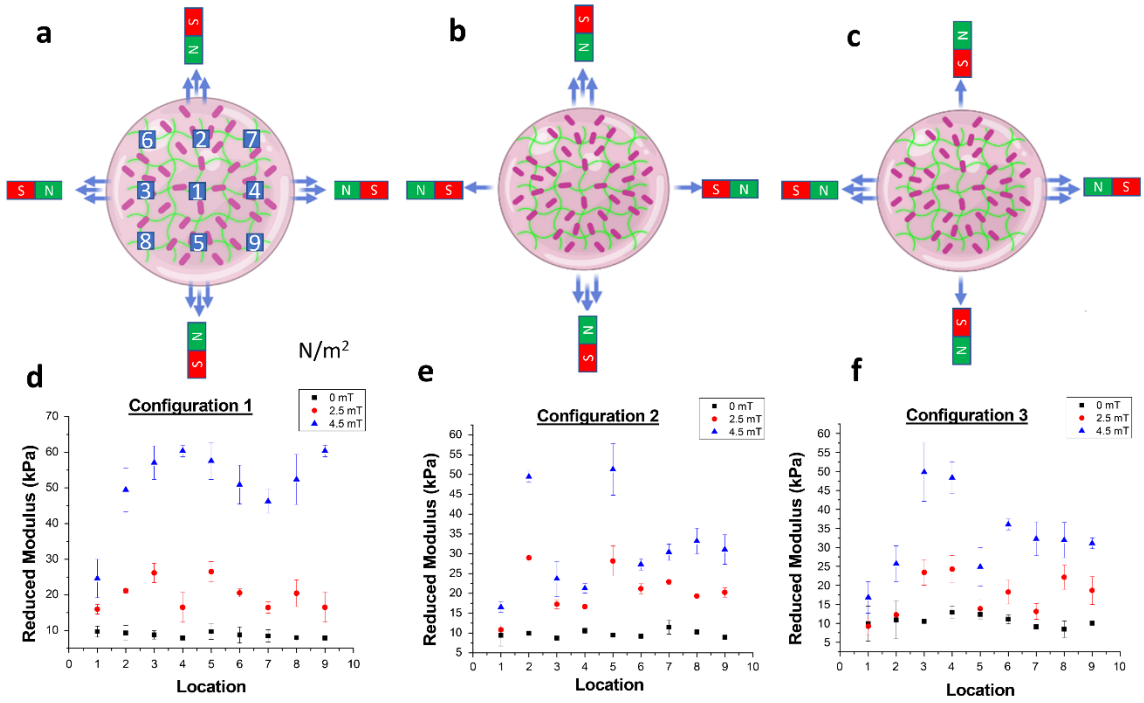

Figure 3.7. Heterogeneous stiffness change under different polarity configurations of the applied magnetic fields. Schematics showing different configurations of the applied magnetic fields and corresponding stiffness measurements at various areas. (a) Same polarity configuration (Configuration 1), (b) Alternate polarity configuration (Configuration 2). (c) Alternate polarity configuration (Configuration 3). (d-f) Location-specific change in reduced Young's modulus in response to the polarity configuration and magnitude of the applied magnetic fields.

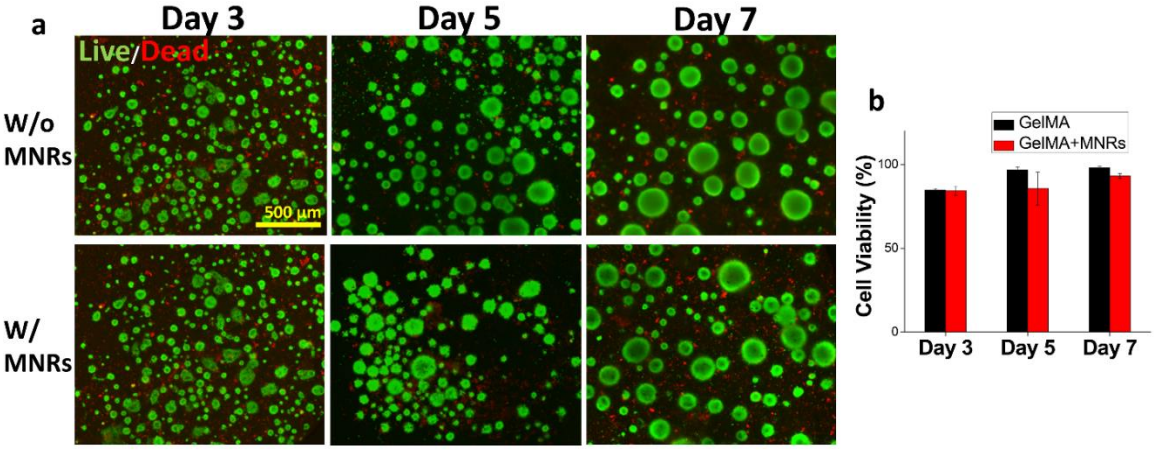

Figure 3.8. Cell viability in the magnetic nanorod (MNR)-incorporated hydrogel. (a) Representative live (green)/dead (red) cell assay images of human induced pluripotent stem cells (iPSCs) cultured within 7.5 wt% gelatin methacrylate (GelMA) with or without MNRs for various durations (scale bar = 500 μm). (b) Quantitative analysis of cell viability in GelMA with or without the incorporation of MNRs ($n = 5$, * and ** denote statistical significance of $p < 0.05$ and $p < 0.01$, respectively.).

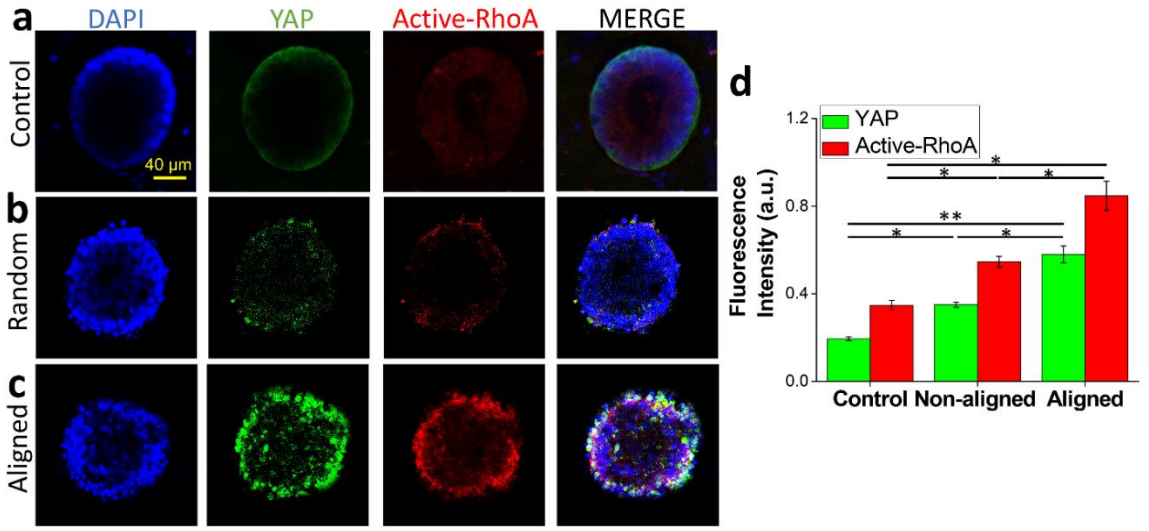

Figure 3.9. The effects of stiffening on the mechano-sensitive Rho/ROCK signaling of human induced pluripotent stem cells (iPSCs) cultured within magnetic nanorod (MNR)-incorporated hydrogel. Representative confocal images of iPSC colonies in the hydrogel (a) without the incorporation of MNRs, (b) with randomly oriented MNRs, or (c) with aligned MNRs, subjected to the applied magnetic field of 4.5 mT for 2 hours (scale bar = 40 μm). (d) Quantification of YAP and active-RhoA fluorescence intensities for various conditions. (n = 5, * and ** denote statistical significance of $p < 0.05$ and $p < 0.01$, respectively.)

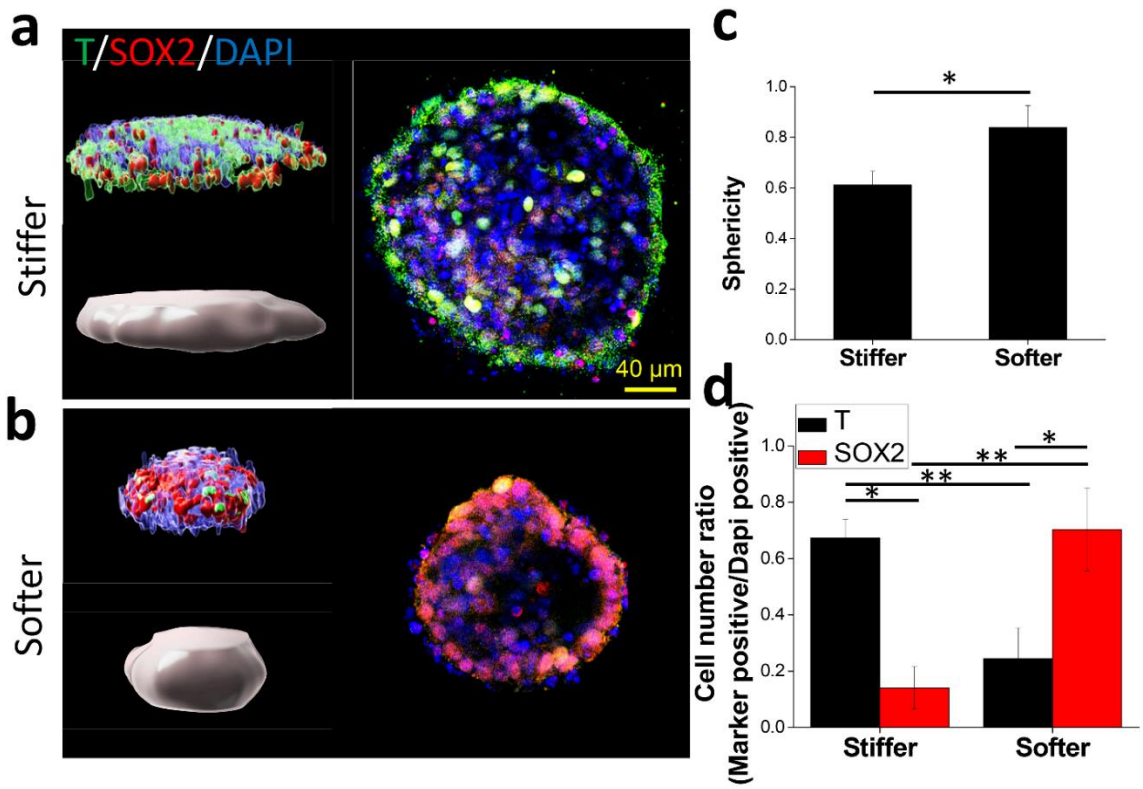

Figure 3.10. The effects of local stiffness on the differentiation of iPSC. Representative confocal images of iPSC colony and its 3D reconstruction in the (a) stiffer and (b) softer regions of hydrogel under the anisotropic application of magnetic fields. (c) Quantification of colony sphericity from 3D reconstruction of iPSC colonies in the stiffer and softer regions of hydrogel. (d) local stiffness-dependent iPSC differentiation quantified from T- and Sox2-positive cells within the 3D iPSC colony within the stiffer and softer regions of the hydrogel (n = 5, * and ** denote statistical significance of $p < 0.05$ and $p < 0.01$, respectively).

CHAPTER 4. CONCLUSIONS

The work presented in this master's thesis provides insight into the effect of the mechano-physical microenvironment on iPSC behaviors. iPSCs that were cultured on electrospun nanofibrous scaffolds system, formed into three-dimensional semispherical colony morphology which exhibited spatially localized distribution patterns of RhoA/ROCK activity, accompanied with the formation of actin-myosin chain, downstream YAP activity, epigenetic regulations as well as heterogenous germ layer differentiation. This work highlighted the role that Rho-ROCK-YAP signaling has on the regulating spatially localized epigenetic modifications as well as subsequent germ layer differentiation. We showed that Rho-ROCK-YAP signaling was activated where the cells experienced the highest amount of stress due to the heterogeneity of the physical microenvironment within the 3D colonies, demonstrating its integral role in mediating the physical environment regulated germ layer differentiation. Additionally, we explored the affects that a magneto-responsive dynamic mechano-modulated hydrogel has on iPSC behavior and differentiation. Rho-ROCK-YAP was activated when stiffness was increased due to MNR attraction towards the magnetic field. Under the control of the anisotropic stiffness field, iPSC colonies within the stiffer region of the hydrogel tended to have a flatter morphology and had more mesendodermal positive cells along the outside of the colonies. In contrast, colonies cultured on the softer region of the hydrogel had a more spherical morphology and had more

ectodermal positive cells inside of the colony with little mesendodermal expression. Furthermore, we demonstrated the role that Rho-ROCK-YAP signaling and how the physical mechano-microenvironment can direct iPSC differentiation and influence subsequent iPSC behaviors. Lastly, we demonstrated the feasibility of utilizing a dynamic magneto-responsive hydrogel to model specific tissue morphogenesis as well as its capabilities in recapitulating the dynamic microenvironments that cells undergo within the cell niche. In future studies this magneto-responsive system can be utilized to study the change in not just iPSC behavior but can also apply dynamic magneto-stiffening towards other cell types as well.

APPENDIX 1. SUPPORTING INFORMATION

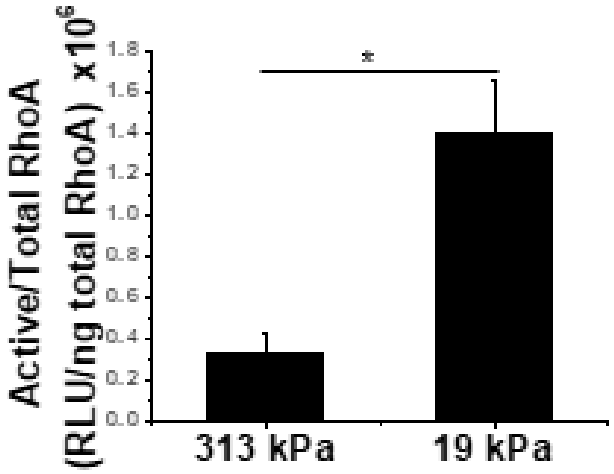

Figure S2.1. Scaffold stiffness dependent RhoA activity.

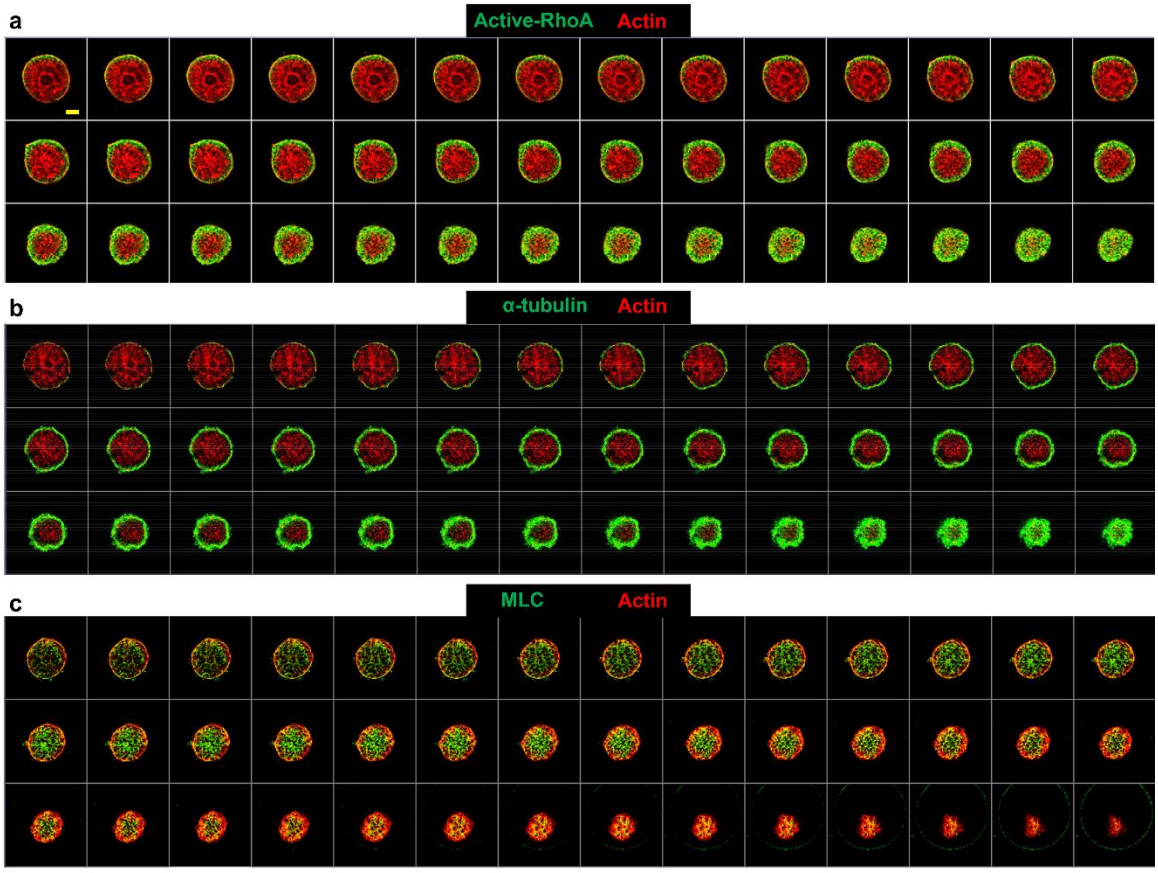

Figure S2.2. Z-stack confocal micrographs of iPSC colonies showing the expression of Active-RhoA (a) and cytoskeleton components (b, c). Scale bar = 50 μm.

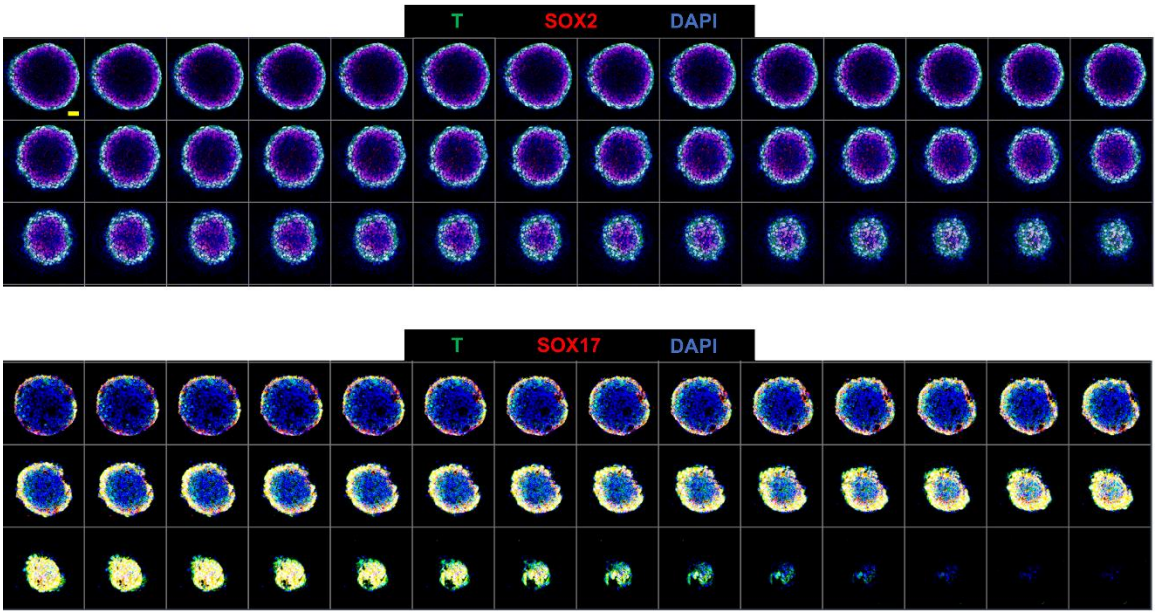

Figure S2.3. Z-stack confocal micrographs showing the distribution of mesendoderm markers (T, SOX17) and extoderm marker (SOX2) inside of the iPSC colonies under BMP4 induced differentiation. Scale bar = 50 μm.

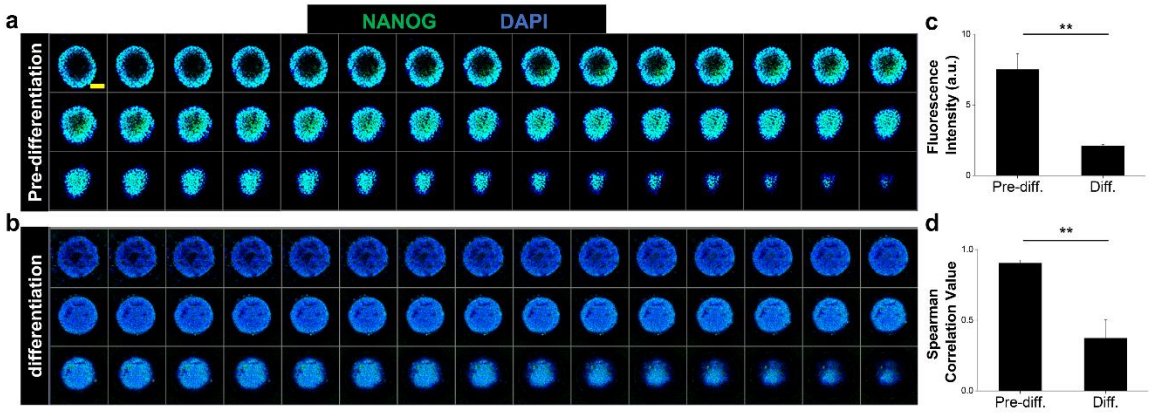

Figure S2.4. (a, b) Z-stack confocal micrographs showing the pluripotency marker NANOG expression under pre-differentiation (a) or differentiation (b) condition. Scale bar = 100 μm. (c, d) Corresponding quantification of fluorescence intensity (c) and NANOG nuclear localization (d). (** denotes $p < 0.01$.)

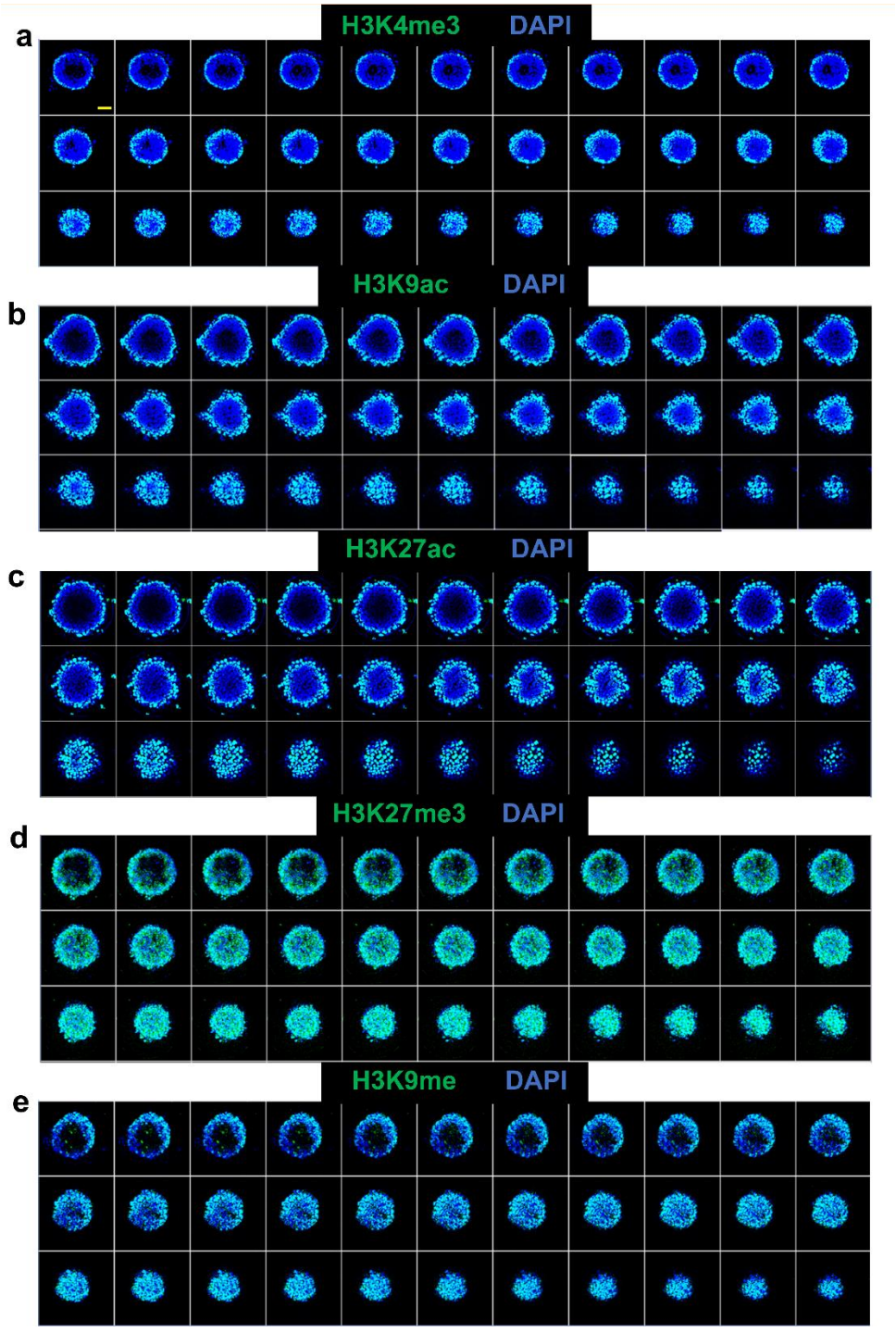

Figure S2.5. Z-stack confocal micrographs showing the localization of epigenetic activities, including H3K4me3 (a), H3K9ac (b), H3K27ac (c), H3K27me3 (d), and H3K9me (e), within the iPSC colonies. Scale bar = 100 μm.

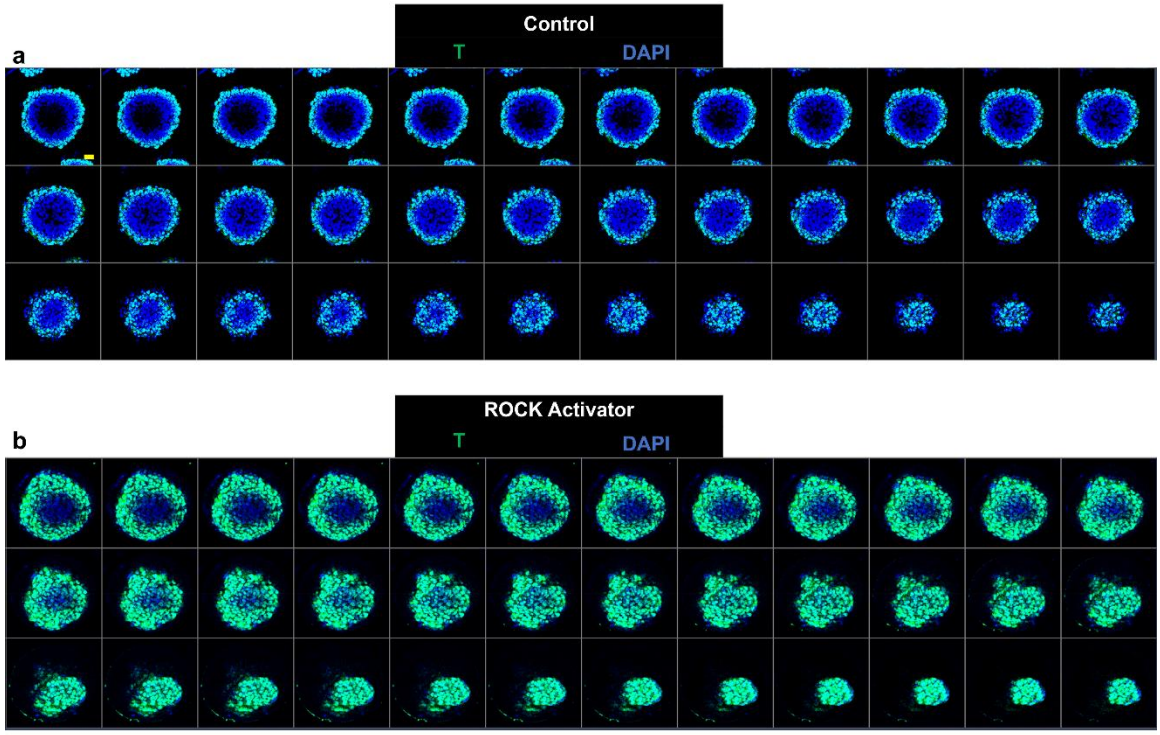

Figure S2.5. Z-stack confocal micrographs showing the distribution of mesendoderm marker T without (a) or with (b) ROCK activator. Scale bar = 50 μm.

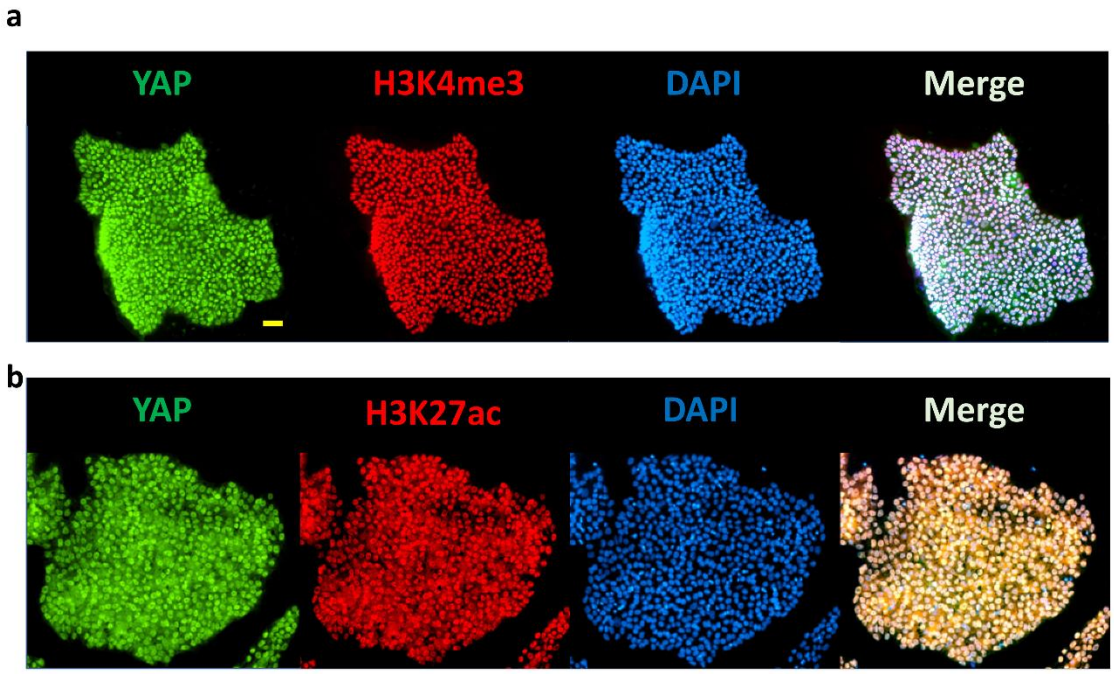

Figure S2.6. Correlation between YAP expression and activating histone modification markers in monolayer iPSC colonies. In pre-differentiation condition, monolayer iPSC colonies tend to express YAP and activating histone modification markers H3K4me3 (A), H3K27ac (B) uniformly and their expression colocalizes in most cells. Scale bar = 20 μm.

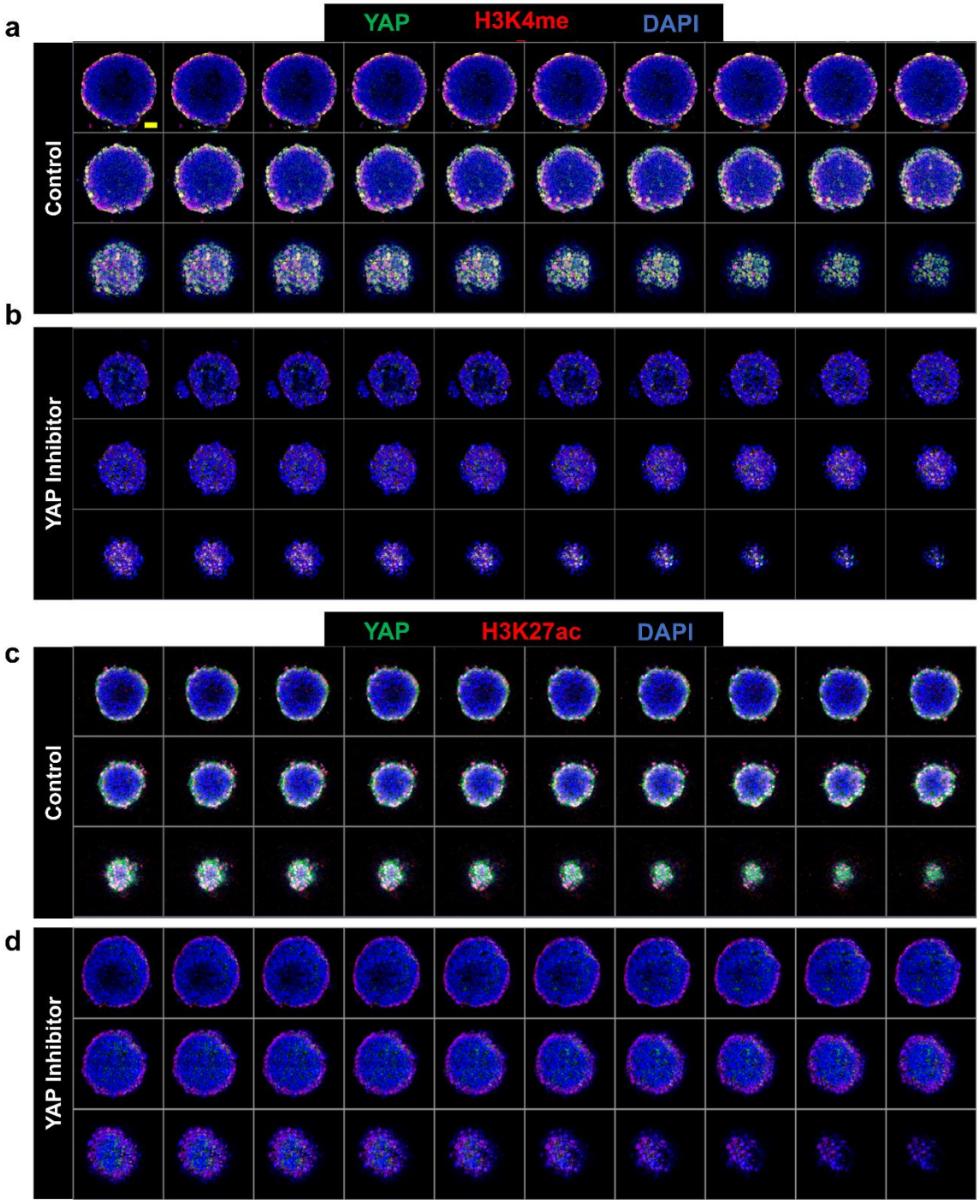

Figure S2.8. Z-stack confocal micrographs showing YAP and epigenetic activities (H3K4me (a, b), and H3K27ac (c, d)) without (a, c) or with (b, d) the application of YAP inhibitor. Scale bar = 50 μm.

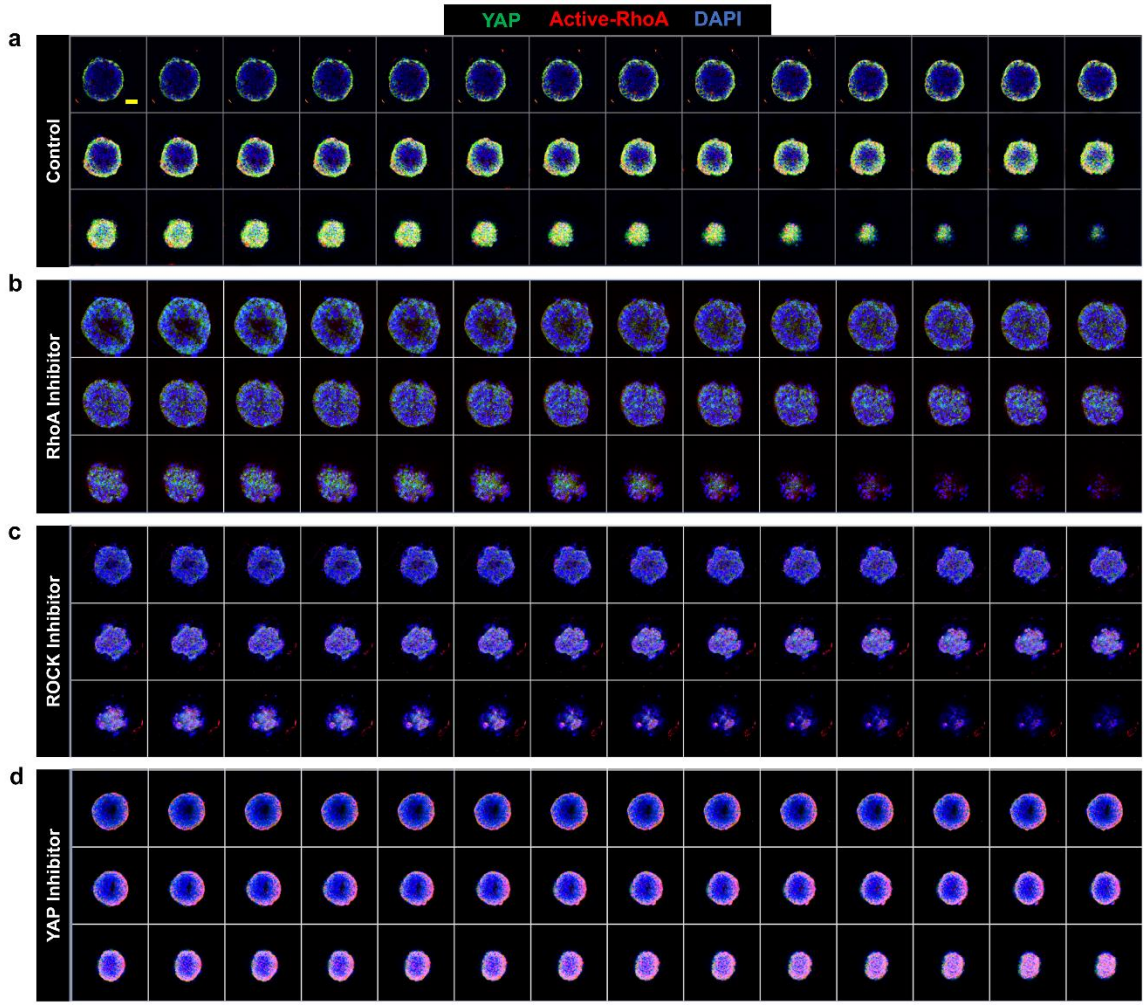

Figure S2.9. Z-stack confocal micrographs showing YAP and Active-RhoA expression in iPSC colonies under various conditions including control (A), RhoA inhibitor (B), ROCK inhibitor (C), and YAP inhibitor (D). Scale bar = 50 μm.

BIBLIOGRAPHY

1. Tai, Y.; Banerjee, A.; Goodrich, R.; Jin, L.; Nam, J., Development and Utilization of Multifunctional Polymeric Scaffolds for the Regulation of Physical Cellular Microenvironments. *Polymers* **2021,** *13* (22), 3880.

2. Maldonado, M.; Ico, G.; Low, K.; Luu, R. J.; Nam, J., Enhanced Lineage-Specific Differentiation Efficiency of Human Induced Pluripotent Stem Cells by Engineering Colony Dimensionality Using Electrospun Scaffolds. *Advanced healthcare materials* **2016,** *5* (12), 1408-1412.

3. Ruedinger, F.; Lavrentieva, A.; Blume, C.; Pepelanova, I.; Scheper, T., Hydrogels for 3D mammalian cell culture: a starting guide for laboratory practice. *Applied microbiology and biotechnology* **2015,** *99* (2), 623-636.

4. Chen, W.; Zhang, Y.; Kumari, J.; Engelkamp, H.; Kouwer, P. H., Magnetic Stiffening in 3D Cell Culture Matrices. *Nano letters* **2021,** *21* (16), 6740-6747.

5. Lin, X.; Shi, Y.; Cao, Y.; Liu, W., Recent progress in stem cell differentiation directed by material and mechanical cues. *Biomedical materials* **2016,** *11* (1), 014109.

6. Ahmed, U.; Ahmed, R.; Masoud, M. S.; Tariq, M.; Ashfaq, U. A.; Augustine, R.; Hasan, A., Stem cells based in vitro models: trends and prospects in biomaterials cytotoxicity studies. *Biomedical Materials* **2021,** *16* (4), 042003.

7. Lee, D. A.; Knight, M. M.; Campbell, J. J.; Bader, D. L., Stem cell mechanobiology. *Journal of cellular biochemistry* **2011,** *112* (1), 1-9.

8. Vining, K. H.; Mooney, D. J., Mechanical forces direct stem cell behaviour in development and regeneration. *Nature reviews Molecular cell biology* **2017,** *18* (12), 728-742.

9. Naqvi, S.; McNamara, L., Stem cell mechanobiology and the role of biomaterials in governing mechanotransduction and matrix production for tissue regeneration. *Frontiers in Bioengineering and Biotechnology* **2020**, 1375.

10. Petridou, N. I.; Heisenberg, C. P., Tissue rheology in embryonic organization. *The EMBO journal* **2019,** *38* (20), e102497.

11. Thompson, A. J.; Pillai, E. K.; Dimov, I. B.; Foster, S. K.; Holt, C. E.; Franze, K., Rapid changes in tissue mechanics regulate cell behaviour in the developing embryonic brain. *Elife* **2019,** *8*, e39356.

12. Kim, T. H.; An, D. B.; Oh, S. H.; Kang, M. K.; Song, H. H.; Lee, J. H., Creating stiffness gradient polyvinyl alcohol hydrogel using a simple gradual freezing–thawing method to investigate stem cell differentiation behaviors. *Biomaterials* **2015,** *40*, 51-60.

13. Zhu, Y.; Li, X.; Janairo, R. R. R.; Kwong, G.; Tsou, A. D.; Chu, J. S.; Wang, A.; Yu, J.; Wang, D.; Li, S., Matrix stiffness modulates the differentiation of neural crest stem cells in vivo. *Journal of Cellular Physiology* **2019,** *234* (5), 7569-7578.

14. Shih, Y. R. V.; Tseng, K. F.; Lai, H. Y.; Lin, C. H.; Lee, O. K., Matrix stiffness regulation of integrin-mediated mechanotransduction during osteogenic differentiation of human mesenchymal stem cells. *Journal of bone and mineral research* **2011,** *26* (4), 730-738.

15. Parrotta, E. I.; Procopio, A.; Scalise, S.; Esposito, C.; Nicoletta, G.; Santamaria, G.; De Angelis, M. T.; Dorn, T.; Moretti, A.; Laugwitz, K.-L., Deciphering the Role of Wnt and Rho Signaling Pathway in iPSC-Derived ARVC Cardiomyocytes by In Silico Mathematical Modeling. *International journal of molecular sciences* **2021,** *22* (4), 2004.

16. Hamada, H. In *Role of physical forces in embryonic development*, Seminars in cell & developmental biology, Elsevier: 2015; pp 88-91.

17. Valet, M.; Siggia, E. D.; Brivanlou, A. H., Mechanical regulation of early vertebrate embryogenesis. *Nature Reviews Molecular Cell Biology* **2021**, 1-16.

18. Dado, D.; Sagi, M.; Levenberg, S.; Zemel, A., Mechanical control of stem cell differentiation. *Regenerative medicine* **2012,** *7* (1), 101-116.

19. Duval, K.; Grover, H.; Han, L.-H.; Mou, Y.; Pegoraro, A. F.; Fredberg, J.; Chen, Z., Modeling physiological events in 2D vs. 3D cell culture. *Physiology* **2017,** *32* (4), 266-277.

20. Ravi, M.; Paramesh, V.; Kaviya, S.; Anuradha, E.; Solomon, F. P., 3D cell culture systems: advantages and applications. *Journal of cellular physiology* **2015,** *230* (1), 16-26.

21. Edmondson, R.; Broglie, J. J.; Adcock, A. F.; Yang, L., Three-dimensional cell culture systems and their applications in drug discovery and cell-based biosensors. *Assay and drug development technologies* **2014,** *12* (4), 207-218.

22. Sankar, S.; Sharma, C. S.; Rath, S. N.; Ramakrishna, S., Electrospun fibers for recruitment and differentiation of stem cells in regenerative medicine. *Biotechnology journal* **2017,** *12* (12), 1700263.

23. Sill, T. J.; Von Recum, H. A., Electrospinning: applications in drug delivery and tissue engineering. *Biomaterials* **2008,** *29* (13), 1989-2006.

24. Prabhakaran, M. P.; Venugopal, J.; Ghasemi-Mobarakeh, L.; Kai, D.; Jin, G.; Ramakrishna, S., Stem cells and nanostructures for advanced tissue regeneration. *Biomedical applications of polymeric nanofibers* **2011**, 21-62.

25. Maldonado, M.; Wong, L. Y.; Echeverria, C.; Ico, G.; Low, K.; Fujimoto, T.; Johnson, J. K.; Nam, J., The effects of electrospun substrate-mediated cell colony morphology on the self-renewal of human induced pluripotent stem cells. *Biomaterials* **2015,** *50*, 10-19.

26. Lin, C.; Liu, C.; Zhang, L.; Huang, Z.; Zhao, P.; Chen, R.; Pang, M.; Chen, Z.; He, L.; Luo, C., Interaction of iPSC-derived neural stem cells on poly (L-lactic acid) nanofibrous scaffolds for possible use in neural tissue engineering. *international journal of molecular medicine* **2018,** *41* (2), 697-708.

27. Mahboudi, H.; Soleimani, M.; Enderami, S. E.; Kehtari, M.; Hanaee-Ahvaz, H.; Ghanbarian, H.; Bandehpour, M.; Nojehdehi, S.; Mirzaei, S.; Kazemi, B., The effect of nanofibre-based polyethersulfone (PES) scaffold on the chondrogenesis of human induced pluripotent stem cells. *Artificial cells, nanomedicine, and biotechnology* **2018,** *46* (8), 1948-1956.

28. Vats, K.; Benoit, D. S., Dynamic manipulation of hydrogels to control cell behavior: a review. *Tissue Engineering Part B: Reviews* **2013,** *19* (6), 455-469.

29. Lieleg, O.; Ribbeck, K., Biological hydrogels as selective diffusion barriers. *Trends in cell biology* **2011,** *21* (9), 543-551.

30. Wu, S.; Xu, R.; Duan, B.; Jiang, P., Three-dimensional hyaluronic acid hydrogel-based models for in vitro human iPSC-derived NPC culture and differentiation. *Journal of Materials Chemistry B* **2017,** *5* (21), 3870-3878.

31. Luo, Y.; Lou, C.; Zhang, S.; Zhu, Z.; Xing, Q.; Wang, P.; Liu, T.; Liu, H.; Li, C.; Shi, W., Three-dimensional hydrogel culture conditions promote the differentiation of human induced pluripotent stem cells into hepatocytes. *Cytotherapy* **2018,** *20* (1), 95-107.

32. Prauzner-Bechcicki, S.; Raczkowska, J.; Madej, E.; Pabijan, J.; Lukes, J.; Sepitka, J.; Rysz, J.; Awsiuk, K.; Bernasik, A.; Budkowski, A., PDMS substrate stiffness affects the morphology and growth profiles of cancerous prostate and melanoma cells. *Journal of the mechanical behavior of biomedical materials* **2015,** *41*, 13-22.

33. Bhagat, A. A. S.; Jothimuthu, P.; Papautsky, I., Photodefinable

polydimethylsiloxane (PDMS) for rapid lab-on-a-chip prototyping. *Lab on a Chip* **2007,** *7* (9), 1192-1197.

34. De Silva, M. N.; Desai, R.; Odde, D. J., Micro-patterning of animal cells on PDMS substrates in the presence of serum without use of adhesion inhibitors. *Biomedical microdevices* **2004,** *6* (3), 219.

35. Lee, H.; Kim, G. M.; Choi, J. H.; Park, M. H.; Bae, J.-s.; Jin, H. K., Highly efficient reprogramming and characterization of induced pluripotent stem cells by using a microwell array. *Tissue engineering and regenerative medicine* **2016,** *13* (6), 691-700.

36. Tran, R.; Moraes, C.; Hoesli, C. A., Controlled clustering enhances PDX1 and NKX6. 1 expression in pancreatic endoderm cells derived from pluripotent stem cells. *Scientific reports* **2020,** *10* (1), 1-12.

37. Huebsch, N.; Arany, P. R.; Mao, A. S.; Shvartsman, D.; Ali, O. A.; Bencherif, S. A.; Rivera-Feliciano, J.; Mooney, D. J., Harnessing traction-mediated manipulation of the cell/matrix interface to control stem-cell fate. *Nature materials* **2010,** *9* (6), 518-526.

38. Horner, C. B.; Hirota, K.; Liu, J.; Maldonado, M.; Hyle Park, B.; Nam, J., Magnitude-dependent and inversely-related osteogenic/chondrogenic differentiation of human mesenchymal stem cells under dynamic compressive strain. *Journal of tissue engineering and regenerative medicine* **2018,** *12* (2), e637-e647.

39. Bryant, S. J.; Anseth, K. S.; Lee, D. A.; Bader, D. L., Crosslinking density influences the morphology of chondrocytes photoencapsulated in PEG hydrogels during the application of compressive strain. *Journal of Orthopaedic Research* **2004,** *22* (5), 1143-1149.

40. Marędziak, M.; Śmieszek, A.; Tomaszewski, K. A.; Lewandowski, D.; Marycz, K., The effect of low static magnetic field on osteogenic and adipogenic differentiation potential of human adipose stromal/stem cells. *Journal of Magnetism and Magnetic Materials* **2016,** *398*, 235-245.

41. Kannarkat, J. T.; Battogtokh, J.; Philip, J.; Wilson, O. C.; Mehl, P. M., Embedding of magnetic nanoparticles in polycaprolactone nanofiber scaffolds to facilitate bone healing and regeneration. *Journal of Applied Physics* **2010,** *107* (9), 09B307.

42. Kim, J.-J.; Singh, R. K.; Seo, S.-J.; Kim, T.-H.; Kim, J.-H.; Lee, E.-J.; Kim, H.-W., Magnetic scaffolds of polycaprolactone with functionalized magnetite nanoparticles: physicochemical, mechanical, and biological properties effective for

bone regeneration. *Rsc Advances* **2014,** *4* (33), 17325-17336.

43. Ross, C. L., The use of electric, magnetic, and electromagnetic field for directed cell migration and adhesion in regenerative medicine. *Biotechnology progress* **2017,** *33* (1), 5-16.

44. Sapir-Lekhovitser, Y.; Rotenberg, M. Y.; Jopp, J.; Friedman, G.; Polyak, B.; Cohen, S., Magnetically actuated tissue engineered scaffold: insights into mechanism of physical stimulation. *Nanoscale* **2016,** *8* (6), 3386-3399.

45. Leulmi, S.; Chauchet, X.; Morcrette, M.; Ortiz, G.; Joisten, H.; Sabon, P.; Livache, T.; Hou, Y.; Carrière, M.; Lequien, S., Triggering the apoptosis of targeted human renal cancer cells by the vibration of anisotropic magnetic particles attached to the cell membrane. *Nanoscale* **2015,** *7* (38), 15904-15914.

46. Gonçalves, A. I.; Rodrigues, M. T.; Carvalho, P. P.; Bañobre-López, M.; Paz, E.; Freitas, P.; Gomes, M. E., Exploring the potential of starch/polycaprolactone aligned magnetic responsive scaffolds for tendon regeneration. *Advanced healthcare materials* **2016,** *5* (2), 213-222.

47. Liu, Z.; Zhu, S.; Liu, L.; Ge, J.; Huang, L.; Sun, Z.; Zeng, W.; Huang, J.; Luo, Z., A magnetically responsive nanocomposite scaffold combined with Schwann cells promotes sciatic nerve regeneration upon exposure to magnetic field. *International Journal of Nanomedicine* **2017,** *12*, 7815.

48. Li, D.; Zhou, J. X.; Chowdhury, F.; Cheng, J. J.; Wang, N.; Wang, F., Role of mechanical factors in fate decisions of stem cells. *Regen Med* **2011,** *6* (2), 229-240.

49. Carpenedo, R. L.; Kwon, S. Y.; Tanner, R. M.; Yockell-Lelievre, J.; Choey, C.; Dore, C.; Ho, M.; Stewart, D. J.; Perkins, T. J.; Stanford, W. L., Transcriptomically Guided Mesendoderm Induction of Human Pluripotent Stem Cells Using a Systematically Defined Culture Scheme. *Stem Cell Rep* **2019,** *13* (6), 1111-1125.

50. Chambers, S. M.; Fasano, C. A.; Papapetrou, E. P.; Tomishima, M.; Sadelain, M.; Studer, L., Highly efficient neural conversion of human ES and iPS cells by dual inhibition of SMAD signaling. *Nat Biotechnol* **2009,** *27* (3), 275-280.

51. Li, J.; Liu, Y.; Zhang, Y.; Yao, B.; Enhejirigala; Li, Z.; Song, W.; Wang, Y.; Duan, X.; Yuan, X.; Fu, X.; Huang, S., Biophysical and Biochemical Cues of Biomaterials Guide Mesenchymal Stem Cell Behaviors. *Front Cell Dev Biol* **2021,** *9*, 640388.

52. Vining, K. H.; Mooney, D. J., Mechanical forces direct stem cell behaviour

in development and regeneration. *Nat Rev Mol Cell Biol* **2017,** *18* (12), 728-742.

53. Minn, K. T.; Fu, Y. C.; He, S.; Dietmann, S.; George, S. C.; Anastasio, M. A.; Morris, S. A.; Solnica-Krezel, L., High-resolution transcriptional and morphogenetic profiling of cells from micropatterned human ESC gastruloid cultures. *Elife* **2020,** *9*.

54. Poh, Y. C.; Chen, J. W.; Hong, Y.; Yi, H. Y.; Zhang, S.; Chen, J. J.; Wu, D. C.; Wang, L. L.; Jia, Q.; Singh, R.; Yao, W. T.; Tan, Y. H.; Tajik, A.; Tanaka, T. S.; Wang, N., Generation of organized germ layers from a single mouse embryonic stem cell. *Nat Commun* **2014,** *5*.

55. Zhang, Y.; Gordon, A.; Qian, W. Y.; Chen, W. Q., Engineering Nanoscale Stem Cell Niche: Direct Stem Cell Behavior at Cell-Matrix Interface. *Advanced Healthcare Materials* **2015,** *4* (13), 1900-1914.

56. Martins, R. P.; Finan, J. D.; Guilak, F.; Lee, D. A., Mechanical regulation of nuclear structure and function. *Annu Rev Biomed Eng* **2012,** *14*, 431-55.

57. Song, Y.; Soto, J.; Li, S., Mechanical regulation of histone modifications and cell plasticity. *Curr Opin Solid State Mater Sci* **2020,** *24* (6).

58. Passaro, F.; De Martino, I.; Zambelli, F.; Di Benedetto, G.; Barbato, M.; D'Erchia, A. M.; Manzari, C.; Pesole, G.; Mutarelli, M.; Cacchiarelli, D.; Antonini, D.; Parisi, S.; Russo, T., YAP contributes to DNA methylation remodeling upon mouse embryonic stem cell differentiation. *J Biol Chem* **2021,** *296*, 100138.

59. Lopez-Hernandez, A.; Sberna, S.; Campaner, S., Emerging Principles in the Transcriptional Control by YAP and TAZ. *Cancers* **2021,** *13* (16).

60. Maldonado, M.; Wong, L. Y.; Echeverria, C.; Ico, G.; Low, K.; Fujimoto, T.; Johnson, J. K.; Nam, J., The effects of electrospun substrate-mediated cell colony morphology on the self-renewal of human induced pluripotent stem cells. *Biomaterials* **2015,** *50*, 10-9.

61. Maldonado, M.; Ico, G.; Low, K.; Luu, R. J.; Nam, J., Enhanced Lineage-Specific Differentiation Efficiency of Human Induced Pluripotent Stem Cells by Engineering Colony Dimensionality Using Electrospun Scaffolds. *Adv Healthc Mater* **2016,** *5* (12), 1408-1412.

62. Maldonado, M.; Luu, R. J.; Ico, G.; Ospina, A.; Myung, D.; Shih, H. P.; Nam, J., Lineage-and developmental stage-specific mechanomodulation of induced pluripotent stem cell differentiation. *Stem cell research & therapy* **2017,** *8* (1), 1-7.

63. Maharam, E.; Yaport, M.; Villanueva, N. L.; Akinyibi, T.; Laudier, D.; He, Z. Y.; Leong, D. J.; Sun, H. B., Rho/Rock signal transduction pathway is required for MSC tenogenic differentiation. *Bone Res* **2015,** *3*.

64. Gu, H.; Yu, S. P.; Gutekunst, C. A.; Gross, R. E.; Wei, L., Inhibition of the Rho signaling pathway improves neurite outgrowth and neuronal differentiation of mouse neural stem cells. *Int J Physiol Pathophysiol Pharmacol* **2013,** *5* (1), 11-20.

65. Chew, T. L.; Masaracchia, R. A.; Goeckeler, Z. M.; Wysolmerski, R. B., Phosphorylation of non-muscle myosin II regulatory light chain by p21-activated kinase (gamma-PAK). *J Muscle Res Cell Motil* **1998,** *19* (8), 839-54.

66. Kassianidou, E.; Hughes, J. H.; Kumar, S., Activation of ROCK and MLCK tunes regional stress fiber formation and mechanics via preferential myosin light chain phosphorylation. *Mol Biol Cell* **2017,** *28* (26), 3832-3843.

67. Kampourakis, T.; Sun, Y. B.; Irving, M., Myosin light chain phosphorylation enhances contraction of heart muscle via structural changes in both thick and thin filaments. *P Natl Acad Sci USA* **2016,** *113* (21), E3039-E3047.

68. Boraas, L. C.; Pineda, E. T.; Ahsan, T., Actin and myosin II modulate differentiation of pluripotent stem cells. *Plos One* **2018,** *13* (4).

69. Maldonado, M.; Luu, R. J.; Ramos, M. E.; Nam, J., ROCK inhibitor primes human induced pluripotent stem cells to selectively differentiate towards mesendodermal lineage via epithelial-mesenchymal transition-like modulation. *Stem Cell Res* **2016,** *17* (2), 222-227.

70. Vallier, L.; Touboul, T.; Chng, Z.; Brimpari, M.; Hannan, N.; Millan, E.; Smithers, L. E.; Trotter, M.; Rugg-Gunn, P.; Weber, A.; Pedersen, R. A., Early cell fate decisions of human embryonic stem cells and mouse epiblast stem cells are controlled by the same signalling pathways. *Plos One* **2009,** *4* (6), e6082.

71. Zhu, S.; Liu, L.; Korzh, V.; Gong, Z.; Low, B. C., RhoA acts downstream of Wnt5 and Wnt11 to regulate convergence and extension movements by involving effectors Rho kinase and Diaphanous: use of zebrafish as an in vivo model for GTPase signaling. *Cellular signalling* **2006,** *18* (3), 359-372.

72. Elosegui-Artola, A.; Andreu, I.; Beedle, A. E.; Lezamiz, A.; Uroz, M.; Kosmalska, A. J.; Oria, R.; Kechagia, J. Z.; Rico-Lastres, P.; Le Roux, A.-L., Force triggers YAP nuclear entry by regulating transport across nuclear pores. *Cell* **2017,** *171* (6), 1397-1410. e14.

73. Desiraju, G. R.; Hulliger, J., Current opinion in solid state & materials science molecular crystals and materials. *Curr Opin Solid St M* **2001,** *5* (2-3), 105-

106.

74. Passaro, F.; Martino, I. D.; Zambelli, F.; Di Benedetto, G.; Barbato, M.; D'Erchia, A. M.; Manzari, C.; Pesole, G.; Mutarelli, M.; Cacchiarelli, D.; Antonini, D.; Parisi, S.; Russo, T., YAP contributes to DNA methylation remodeling upon mouse embryonic stem cell differentiation. *J Biol Chem* **2021,** *296*.

75. Motomura, K.; Okada, N.; Morita, H.; Hara, M.; Tamari, M.; Orimo, K.; Matsuda, G.; Imadome, K. I.; Matsuda, A.; Nagamatsu, T.; Fujieda, M.; Sago, H.; Saito, H.; Matsumoto, K., A Rho-associated coiled-coil containing kinases (ROCK) inhibitor, Y-27632, enhances adhesion, viability and differentiation of human term placenta-derived trophoblasts in vitro. *Plos One* **2017,** *12* (5).

76. Schaumann, E. N.; Staddon, M. F.; Gardel, M. L.; Banerjee, S., Force localization modes in dynamic epithelial colonies. *Mol Biol Cell* **2018,** *29* (23), 2835-2847.

77. Lekka, M.; Gnanachandran, K.; Kubiak, A.; Zielinski, T.; Zemla, J., Traction force microscopy - Measuring the forces exerted by cells. *Micron* **2021,** *150*.

78. Goncalves, A. I.; Rodrigues, M. T.; Lee, S. J.; Atala, A.; Yoo, J. J.; Reis, R. L.; Gomes, M. E., Understanding the role of growth factors in modulating stem cell tenogenesis. *PLoS One* **2013,** *8* (12), e83734.

79. Clause, K. C.; Liu, L. J.; Tobita, K., Directed stem cell differentiation: the role of physical forces. *Cell Commun Adhes* **2010,** *17* (2), 48-54.

80. Discher, D. E.; Mooney, D. J.; Zandstra, P. W., Growth factors, matrices, and forces combine and control stem cells. *Science* **2009,** *324* (5935), 1673-7.

81. Perestrelo, T.; Correia, M.; Ramalho-Santos, J.; Wirtz, D., Metabolic and Mechanical Cues Regulating Pluripotent Stem Cell Fate. *Trends Cell Biol* **2018,** *28* (12), 1014-1029.

82. Li, S.; Yang, D.; Gao, L.; Wang, Y.; Peng, Q., Epigenetic regulation and mechanobiology. *Biophysics Reports* **2020,** *6* (2), 33-48.

83. Godini, R.; Lafta, H. Y.; Fallahi, H., Epigenetic modifications in the embryonic and induced pluripotent stem cells. *Gene Expr Patterns* **2018,** *29*, 1-9.

84. Breuls, N.; Giarratana, N.; Yedigaryan, L.; Sampaolesi, M., Epigenetic modifications in induced pluripotent stem cells to boost myogenic commitment. In *Current Topics in iPSCs Technology*, Elsevier: 2022; pp 197-223.

85. Muncie, J. M.; Ayad, N. M. E.; Lakins, J. N.; Xue, X. F.; Fu, J. P.; Weaver, V. M., Mechanical Tension Promotes Formation of Gastrulation-like Nodes and Patterns Mesoderm Specification in Human Embryonic Stem Cells. *Dev Cell* **2020,** *55* (6), 679-+.

86. Edmondson, R.; Broglie, J. J.; Adcock, A. F.; Yang, L. J., Three-Dimensional Cell Culture Systems and Their Applications in Drug Discovery and Cell-Based Biosensors. *Assay Drug Dev Techn* **2014,** *12* (4), 207-218.

87. Elosegui-Artola, A.; Andreu, I.; Beedle, A. E. M.; Lezamiz, A.; Uroz, M.; Kosmalska, A. J.; Oria, R.; Kechagia, J. Z.; Rico-Lastres, P.; Le Roux, A. L.; Shanahan, C. M.; Trepat, X.; Navajas, D.; Garcia-Manyes, S.; Roca-Cusachs, P., Force Triggers YAP Nuclear Entry by Regulating Transport across Nuclear Pores. *Cell* **2017,** *171* (6), 1397-1410 e14.

88. Kim, C., Disease modeling and cell based therapy with iPSC: future therapeutic option with fast and safe application. *Blood research* **2014,** *49* (1), 7-14.

89. Liao, S. M., Rescuing human embryonic stem cell research: the blastocyst transfer method. *The American Journal of Bioethics* **2005,** *5* (6), 8-16.

90. Nowlan, N. C.; Sharpe, J.; Roddy, K. A.; Prendergast, P. J.; Murphy, P., Mechanobiology of embryonic skeletal development: insights from animal models. *Birth Defects Research Part C: Embryo Today: Reviews* **2010,** *90* (3), 203-213.

91. Hall, B. K.; Herring, S., Paralysis and growth of the musculoskeletal system in the embryonic chick. *Journal of morphology* **1990,** *206* (1), 45-56.

92. Ma, P.; Schloo, B.; Mooney, D.; Langer, R., Development of biomechanical properties and morphogenesis of in vitro tissue engineered cartilage. *Journal of biomedical materials research* **1995,** *29* (12), 1587-1595.

93. Nam, J.; Perera, P.; Rath, B.; Agarwal, S., Dynamic regulation of bone morphogenetic proteins in engineered osteochondral constructs by biomechanical stimulation. *Tissue engineering Part A* **2013,** *19* (5-6), 783-792.

94. Tsata, V.; Beis, D., In full force. Mechanotransduction and morphogenesis during homeostasis and tissue regeneration. *Journal of Cardiovascular Development and Disease* **2020,** *7* (4), 40.

95. Voog, J.; Jones, D. L., Stem cells and the niche: a dynamic duo. *Cell stem cell* **2010,** *6* (2), 103-115.

96. Schneider, R. K.; Anraths, J.; Kramann, R.; Bornemann, J.; Bovi, M.;

Knüchel, R.; Neuss, S., The role of biomaterials in the direction of mesenchymal stem cell properties and extracellular matrix remodelling in dermal tissue engineering. *Biomaterials* **2010,** *31* (31), 7948-7959.

97. Stowers, R. S.; Allen, S. C.; Suggs, L. J., Dynamic phototuning of 3D hydrogel stiffness. *Proceedings of the National Academy of Sciences* **2015,** *112* (7), 1953-1958.

98. Hackelbusch, S.; Rossow, T.; Steinhilber, D.; Weitz, D. A.; Seiffert, S., Hybrid microgels with thermo-tunable elasticity for controllable cell confinement. *Advanced Healthcare Materials* **2015,** *4* (12), 1841-1848.

99. Yan, T.; Rao, D.; Chen, Y.; Wang, Y.; Zhang, Q.; Wu, S., Magnetic nanocomposite hydrogel with tunable stiffness for probing cellular responses to matrix stiffening. *Acta biomaterialia* **2022,** *138*, 112-123.

100. NORIMURA, T.; IMADA, H.; KUNUGITA, N.; YOSHIDA, N.; NIKAIDO, M., Effects of strong magnetic fields on cell growth and radiation response of human T-lymphocytes in culture. *Journal of UOEH* **1993,** *15* (2), 103-112.

101. Torrez, L. B.; Perez, Y.; Yang, J.; Zur Nieden, N. I.; Klassen, H.; Liew, C. G., Derivation of neural progenitors and retinal pigment epithelium from common marmoset and human pluripotent stem cells. *Stem cells international* **2012,** *2012*.

102. Chatterjee, P.; Cheung, Y.; Liew, C., Transfecting and nucleofecting human induced pluripotent stem cells. *JoVE (Journal of Visualized Experiments)* **2011,** (56), e3110.

103. Acevedo-Acevedo, S.; Crone, W. C., Substrate stiffness effect and chromosome missegregation in hIPS cells. *Journal of Negative Results in Biomedicine* **2015,** *14* (1), 1-7.

104. Wheelwright, M.; Win, Z.; Mikkila, J. L.; Amen, K. Y.; Alford, P. W.; Metzger, J. M., Investigation of human iPSC-derived cardiac myocyte functional maturation by single cell traction force microscopy. *PLoS One* **2018,** *13* (4), e0194909.

105. Lv, H.; Wang, H.; Zhang, Z.; Yang, W.; Liu, W.; Li, Y.; Li, L., Biomaterial stiffness determines stem cell fate. *Life sciences* **2017,** *178*, 42-48.

106. Smith, L. R.; Cho, S.; Discher, D. E., Stem cell differentiation is regulated by extracellular matrix mechanics. *Physiology* **2018,** *33* (1), 16-25.

107. Sun, T.; Norton, D.; McKean, R. J.; Haycock, J. W.; Ryan, A. J.; MacNeil, S., Development of a 3D cell culture system for investigating cell interactions with

electrospun fibers. *Biotechnology and bioengineering* **2007,** *97* (5), 1318-1328.

108. Koroleva, A.; Deiwick, A.; El-Tamer, A.; Koch, L.; Shi, Y.; Estévez-Priego, E.; Ludl, A.-A.; Soriano, J.; Guseva, D.; Ponimaskin, E., In vitro development of human iPSC-derived functional neuronal networks on laser-fabricated 3D scaffolds. *ACS Applied Materials & Interfaces* **2021,** *13* (7), 7839-7853.

109. Lin, S.; Gu, L., Influence of crosslink density and stiffness on mechanical properties of type I collagen gel. *Materials* **2015,** *8* (2), 551-560.

110. Jang, J.; Seol, Y.-J.; Kim, H. J.; Kundu, J.; Kim, S. W.; Cho, D.-W., Effects of alginate hydrogel cross-linking density on mechanical and biological behaviors for tissue engineering. *journal of the mechanical behavior of biomedical materials* **2014,** *37*, 69-77.

111. Accardo, J. V.; Kalow, J. A., Reversibly tuning hydrogel stiffness through photocontrolled dynamic covalent crosslinks. *Chemical science* **2018,** *9* (27), 5987-5993.

112. Arkenberg, M. R.; Moore, D. M.; Lin, C.-C., Dynamic control of hydrogel crosslinking via sortase-mediated reversible transpeptidation. *Acta biomaterialia* **2019,** *83*, 83-95.

113. Zheng, Z.; Hu, J.; Wang, H.; Huang, J.; Yu, Y.; Zhang, Q.; Cheng, Y., Dynamic softening or stiffening a supramolecular hydrogel by ultraviolet or near-infrared light. *ACS applied materials & interfaces* **2017,** *9* (29), 24511-24517.

114. Tran, K. A.; Kraus, E.; Clark, A. T.; Bennett, A.; Pogoda, K.; Cheng, X.; Cēbers, A.; Janmey, P. A.; Galie, P. A., Dynamic tuning of viscoelastic hydrogels with carbonyl iron microparticles reveals the rapid response of cells to three-dimensional substrate mechanics. *ACS applied materials & interfaces* **2021,** *13* (18), 20947-20959.

115. Abdeen, A. A.; Lee, J.; Bharadwaj, N. A.; Ewoldt, R. H.; Kilian, K. A., Temporal modulation of stem cell activity using magnetoactive hydrogels. *Advanced healthcare materials* **2016,** *5* (19), 2536-2544.

116. Blyakhman, F. A.; Melnikov, G. Y.; Makarova, E. B.; Fadeyev, F. A.; Sedneva-Lugovets, D. V.; Shabadrov, P. A.; Volchkov, S. O.; Mekhdieva, K. R.; Safronov, A. P.; Fernández Armas, S., Effects of constant magnetic field to the proliferation rate of human fibroblasts grown onto different substrates: Tissue culture polystyrene, polyacrylamide hydrogel and ferrogels γ-Fe2O3 magnetic nanoparticles. *Nanomaterials* **2020,** *10* (9), 1697.

117. Blyakhman, F. A.; Safronov, A. P.; Zubarev, A. Y.; Shklyar, T. F.;

Makeyev, O. G.; Makarova, E. B.; Melekhin, V. V.; Larrañaga, A.; Kurlyandskaya, G. V., Polyacrylamide ferrogels with embedded maghemite nanoparticles for biomedical engineering. *Results in physics* **2017,** *7*, 3624-3633.

118. Kim, S.; Ico, G.; Bai, Y.; Yang, S.; Lee, J.-H.; Yin, Y.; Myung, N. V.; Nam, J., Utilization of a magnetic field-driven microscopic motion for piezoelectric energy harvesting. *Nanoscale* **2019,** *11* (43), 20527-20533.

119. Corbin, E. A.; Vite, A.; Peyster, E. G.; Bhoopalam, M.; Brandimarto, J.; Wang, X.; Bennett, A. I.; Clark, A. T.; Cheng, X.; Turner, K. T., Tunable and reversible substrate stiffness reveals a dynamic mechanosensitivity of cardiomyocytes. *ACS applied materials & interfaces* **2019,** *11* (23), 20603-20614.

120. Zhang, Z.; Liu, M.; Zheng, Y., Role of Rho GTPases in stem cell regulation. *Biochemical Society Transactions* **2021,** *49* (6), 2941-2955.

121. Williams, D. A.; Zheng, Y.; Cancelas, J. A., Rho GTPases and regulation of hematopoietic stem cell localization. *Methods in enzymology* **2008,** *439*, 365-393.